Reversibility of permafrost carbon pool changes under temperature overshoot scenarios

by

Takuma Mihara

BSc, University of Victoria, 2018

Thesis Submitted in Partial Fulfillment of the
Requirements for the Degree of
Master of Science

in the
Department of Geography
Faculty of Environment

SIMON FRASER UNIVERSITY
Fall 2023

Declaration of Committee

Name:	**Takuma Mihara**
Degree:	**Master of Science**
Title:	**Reversibility of permafrost carbon pool changes under temperature overshoot scenarios**
Committee:	**Chair:** **Suzana Dragicevic** Professor, Geography
	Kirsten Zickfeld Supervisor Professor, Geography
	Karen Kohfeld Committee Member Professor, Resource and Environmental Management
	Andrew MacDougall Committee Member Associate Professor, Climate and Environment St. Francis Xavier University
	David Lawrence Examiner Chief Scientist, Terrestrial Sciences National Centre for Atmospheric Research

Abstract

Most pathways that meet the Paris Agreement goal of limiting the global temperature increase to well below 2°C above preindustrial levels will require a temporary exceedance (“overshoot”) of the target temperature. If the target temperature is exceeded, a larger proportion of high-latitude permafrost soils will thaw, releasing additional carbon. The goal of this thesis is to examine whether permafrost carbon loss during the temperature overshoot phase is reversible if the temperature is restored to its target level. To attain this goal, we force an Earth system model of intermediate complexity with a set of scenarios with varying magnitudes and durations of overshoot. Results show that high-latitude soil carbon changes in response to overshoot are dependent on peak warming and the duration of time that excess warming is held. Continued decline of the permafrost region soil carbon pool following temperature restoration suggests that changes are irreversible for at least several centuries.

Keywords: permafrost carbon loss; temperature overshoot

Acknowledgements

I would like to acknowledge Dr. Kirsten Zickfeld for her continuous guidance. Her mentorship during the entire research process from understanding Earth system modelling to using precise wording in my writing has been invaluable to my success.

I would also like to thank Dr. Andrew MacDougall for guiding me through the soil carbon model, and Dr. Karen Kohfeld for proving insight towards my writing. Members of the Climate Lab provided ongoing guidance and a sense of community during my time at SFU, which helped make progress on my research. I'm grateful for all of my friends and family that supported my endeavours in graduate school.

This research was funded by a Natural Sciences and Engineering Research Council of Canada (NSERC) Discovery Grant awarded to Dr. Kirsten Zickfeld.

Table of Contents

List of Figures

Chapter 1. Introduction

Climate change is showing unprecedented environmental impacts such as an increase in the intensity and frequency of extreme weather events, glacier retreat, sea level rise, and permafrost thaw (IPCC, 2023). These impacts will continue to worsen unless anthropogenic greenhouse gas emissions are halted (IPCC, 2021). The primary indicator of climate change is the rise in the global mean surface air temperature (SAT). To avoid the most severe consequences of climate change, the legally binding United Nations Paris Agreement sets the goal to hold "the increase in the global average temperature to well below 2 °C above preindustrial levels" and to pursue efforts "to limit the temperature increase to 1.5 °C above preindustrial levels" (UNFCCC, 2015). Limiting warming to 1.5°C above preindustrial levels has recently been emphasized in the updated Glasgow climate pact (UNFCCC, 2021).

Staying below the 1.5 °C temperature limit requires getting to net zero carbon dioxide (CO_2) emissions by mid-century (IPCC, 2018). Under current policies and pledges, this is virtually impossible, unless transformative action is taken (Meinshausen et al., 2022; Rogelj et al., 2018; C. J. Smith et al., 2019). Most pathways that limit warming to 1.5 °C by the end of the century will require temperature overshoot, where the global mean SAT is restored to a target level after an initial exceedance, using carbon dioxide removal (CDR; IPCC, 2018). CDR is a strategy proposed to sequester atmospheric CO_2 into ocean, terrestrial, or geological reservoirs (National Research Council, 2015). Notable examples of CDR include afforestation/reforestation, bioenergy with carbon capture and storage (BECCS), direct air capture of CO_2 (DAC), enhanced weathering of minerals for carbon storage in soils, land, or the ocean (EW), and enhanced ocean carbon uptake (Smith et al., 2016). If CDR is successfully deployed at large scales, net negative emissions can be achieved when the rate of CO_2 removal surpasses the rate of anthropogenic CO_2 emissions.

The purpose of negative CO_2 emissions is to reverse the effects of climate change, with the reversibility timeline differing for each aspect of the Earth system. SAT warming is known to be reversible almost immediately after net negative CO_2 emissions are reached (Zickfeld et al., 2016). However, other Earth system components take longer to be reversed. Changes can be considered irreversible when the time to return to

a given target level takes multiple centuries, making it irrelevant to human society. For example, ocean heat uptake exhibits a slow response to net negative CO_2 emissions, resulting in thermosteric sea level rise that is irreversible for over a millennium (Ehlert & Zickfeld, 2018; Mengel et al., 2018; Tokarska & Zickfeld, 2015). Regional ocean temperatures and ocean acidification will take several centuries to respond to negative CO_2 emissions (Li et al., 2020). Once weakened, the Atlantic meridional overturning circulation (AMOC) could take several centuries to recover (Jackson & Wood, 2018; Sgubin et al., 2015). The northern high-latitude terrestrial biosphere could retain additional carbon for centuries following negative emissions (Park & Kug, 2022), and carbon lost from permafrost soils could possibly take centuries to millennia to recover (MacDougall & Knutti, 2016). Reversal will have different timescales depending on the process driving the change (Boucher et al., 2012).

Permafrost thaw induced by warming has been observed and is expected to accelerate within the coming decades (Schuur et al., 2022). Because soil temperature change in response to a change in SAT is delayed and attenuated due to the insulating properties of soil, warming generally follows long-term trends rather than year-to-year fluctuations (Biskaborn et al., 2019). This is also expected to hold true when warming is reversed. Permafrost refreeze is found to start 3-4 decades after SAT begins to decline, and to recover a majority of the area that was present before temperature overshoot within a century (Eliseev et al., 2014; Wright, 2020).

However, carbon stored within permafrost soil will not have the same reversibility timeline as physical permafrost extent. The estimated 1460-1600 GtC of soil carbon accumulated from organic matter in the northern circumpolar region (IPCC, 2018), with 1000 GtC (-170, +186) being in the top 0-3 m of soils (Mishra et al., 2021), is at risk of being released into the atmosphere. Soil heterotrophic respiration of thawed permafrost carbon in the Arctic has increased with warming, and is expected to accelerate towards the end of the century (Nissan et al., 2023). The amount of permafrost carbon that will be lost to the atmosphere depends on the warming trajectory (Burke et al., 2018; Gasser et al., 2018).

Modelling studies show that temperature overshoot scenarios will lead to more permafrost carbon release than scenarios that reach a given temperature target without overshoot (de Vrese & Brovkin, 2021; Gasser et al., 2018; Natali et al., 2021). High-

latitude soil temperature and hydrology are slow to respond to atmospheric changes, and could continue to release CO_2 for centuries following temperature stabilization (de Vrese & Brovkin, 2021). Permafrost carbon loss will be highly dependent on the overshoot scenario taken (de Vrese et al., 2021; de Vrese & Brovkin, 2021; Gasser et al., 2018). Loss is directly linked to SAT, and a high overshoot magnitude and duration would release a larger amount of carbon (Schwinger et al., 2022).

Recovery of lost permafrost carbon will likely take centuries to millennia (de Vrese & Brovkin, 2021; MacDougall & Knutti, 2016). Permafrost carbon recovery depends on the rate of cryoturbation, which is the vertical movement rate (in mm/yr) of carbon deeper into the soil column, caused by physical mixing of soil through ice growth and annual freeze-thaw cycles (Bockheim, 2007). Cryoturbation rates are variable, and there is a large degree of uncertainty due to a lack of observations (Jelinski et al., 2017). Nevertheless, the cryoturbation rate is very slow, ranging from 0.1 mm/year (Klaminder et al., 2014) to 1 mm/year (Becher et al., 2013), and the soil organic carbon (SOC) turnover time in permafrost soils is over 1400 years according to models and observations (Shu et al., 2020), suggesting that permafrost carbon loss is likely an irreversible component of the Earth system.

1.1. Research Questions

Recent studies have explored the impacts of climate change scenarios on the permafrost carbon pool using land surface models (Burke et al., 2018; McGuire et al., 2018) and Earth system models of intermediate complexity (EMIC; MacDougall & Knutti, 2016), but few have used overshoot scenarios (de Vrese et al., 2021; de Vrese & Brovkin, 2021; Gasser et al., 2018). There has not been a systematic assessment of how overshoot magnitude and duration impacts permafrost carbon stocks, and whether permafrost carbon loss is reversible on timescales relevant to human society (decades to a century). For the purpose of this thesis, a change is defined as reversible if it recovers to the same level as in a given reference scenario.

This thesis addresses the following research questions:

- On what timescale is permafrost region carbon loss reversible under temperature overshoot scenarios?

- To what extent is the reversibility of permafrost region carbon loss sensitive to the magnitude and duration of overshoot?

The research questions are addressed using an Earth system modelling approach. Following a historical simulation, the model is forced with an ambitious mitigation scenario with temperature overshoot and a set of idealized emission scenarios of varying overshoot magnitudes and duration. Globally averaged and spatially explicit soil carbon variables from the model are analyzed. Resulting outputs show that temperature overshoot leaves long-term legacies in the northern high-latitude carbon pool. A higher peak warming temperature and a longer duration of overshoot leads to more carbon loss from permafrost soils. During the zero-emissions phase following warming and cooling, carbon amounts in the idealized scenarios do not recover to the same level as in the reference scenario for at least several centuries.

The remainder of this thesis includes a methods chapter describing the model used and the scenarios designed to drive the model. A results chapter follows, showing the spatial changes in permafrost area and soil carbon variables, and differences between the overshoot scenarios over time. Next, the discussion chapter addresses the robustness of the results, compares results with similar studies, addresses model and scenario limitations, and policy implications. The thesis concludes with a summary and outlook for future research.

Chapter 2. Methods

2.1. Model Description

The University of Victoria Earth System Climate Model (UVic ESCM) is an Earth system model of intermediate complexity (EMIC) with a grid resolution of 3.6° longitude and 1.8° latitude (Weaver et al., 2001). This study uses model version 2.10 illustrated in Figure 1 (Mengis et al., 2020), which consists of a 2-dimensional energy-moisture balance atmospheric model (Fanning & Weaver, 1996) with dynamical feedbacks, coupled to a 3-dimensional ocean general circulation model (Pacanowski, 1996) with an organic and inorganic carbon cycle (Schmittner et al., 2008), a dynamic-thermodynamic sea-ice model (Bitz & Lipscomb, 1999), a land surface model (Meissner et al., 2003) that includes permafrost (MacDougall & Knutti, 2016), and a dynamic vegetation model that represents the terrestrial carbon cycle (Cox, 2001).

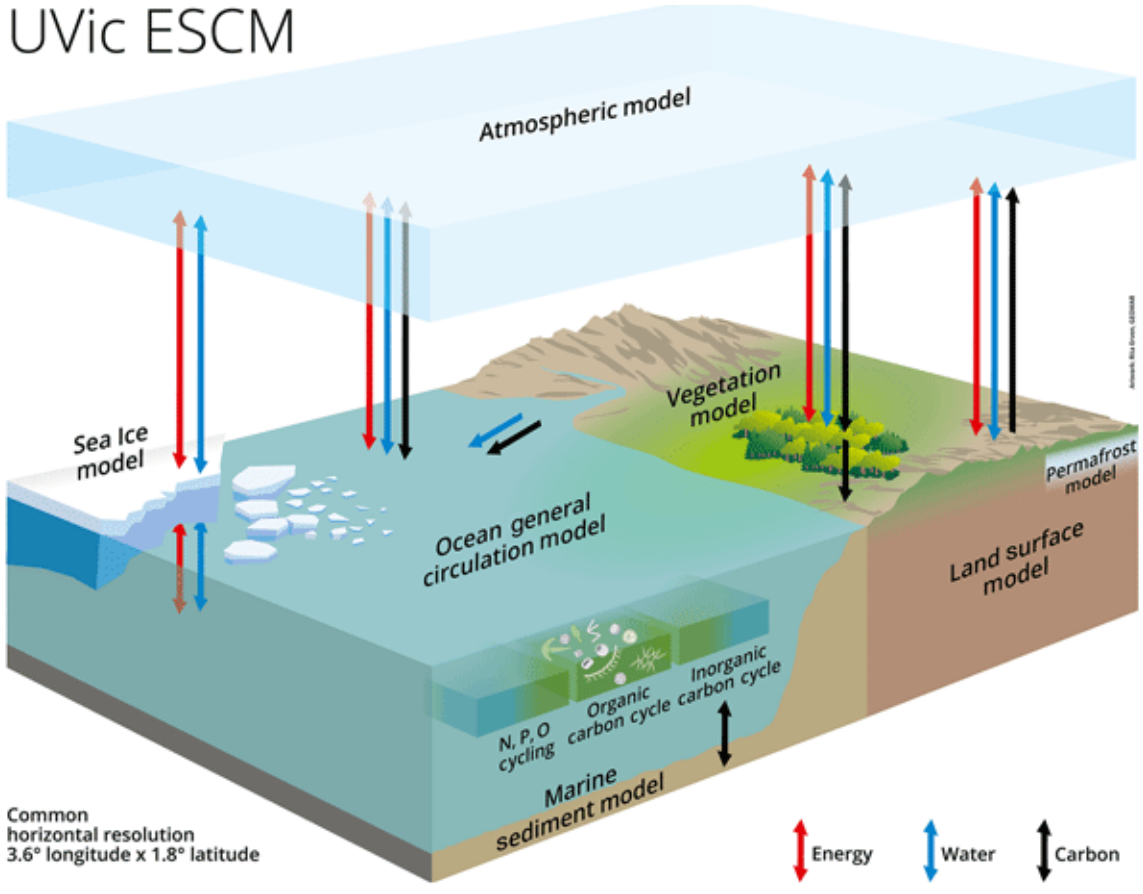

Figure 1 **Schematic of the University of Victoria Earth system climate model version 2.10 (Mengis et al., 2020)**

The land surface model includes 14 subsurface layers, with thickness exponentially increasing with depth (Avis, 2012). The top 8 layers (10 m) are soil layers where moisture can drain freely, and the bottom layers (10-250 m) are granitic bedrock (Avis et al., 2011). Porosity, permeability, and thermal conductivity in the soil layers depend on particle size and organic content (Avis, 2012). Freeze-thaw representation of soil layers allow for permafrost thermal processes to take place. When a soil layer is below freezing for more than two consecutive years, it is classified as permafrost.

The top 6 (0-3.35 m depth) out of the 8 soil layers contain carbon represented as a density or concentration (kg/m^3), which can be defined as near-surface soil carbon. Layers 7 and 8 have the same soil properties as the above layers, but do not contain any carbon. The upper soil layers in the permafrost region that experiences seasonal freeze-thaw cycles as the soil temperature fluctuates past 0 °C are referred to as the active layer. In the UVic ESCM, the active layer typically consists of the top 2-3 soil layers. Permafrost soil begins below the active layer, and the boundary between the active and permafrost layers is called the permafrost table.

Carbon density in the top 6 soil layers is determined by root density for each layer and vegetation litter added to the top layer (MacDougall et al., 2012). Cryoturbation is a mechanical mixing process that distributes soil carbon towards the deeper and colder regions of soil through freeze-thaw cycles (Bockheim, 2007). Cryoturbation involves many complex small-scale processes in the soil that are difficult to capture in large-scale models, and is almost always approximated by diffusion in land surface models (de Vrese et al., 2021). Such a diffusion scheme was developed by Koven et al., (2009) and adapted for the UVic ESCM by MacDougall and Knutti (2016):

$$\frac{\partial C}{\partial t} = K_v \frac{\partial^2 C_{eff}}{\partial z^2} \quad \text{(Equation 1)}$$

The diffusion parameter (K_v, m^2/year) sets the rate of carbon diffusion between layers until a depth (z, in meters) of 3.35 m. Diffusion is carried out using an effective carbon concentration (C_{eff}) for each layer except the first to produce permafrost soil carbon concentrations that diminish with depth. C_{eff} is calculated based on the actual carbon concentration of each layer (C, kg/m^3), the volumetric porosity which diminishes with depth in the model, and a saturation factor for tuning the size of the permafrost carbon pool. Total soil carbon mass generated with this diffusion scheme and its spatial

distribution in the northern high-latitude region has been validated against observations, and is in reasonable agreement (MacDougall & Knutti, 2016).

In this study, the default K_v is set to 5 cm^2/year (0.0005 m^2/year) which is within the range of observation-based studies (Klaminder et al., 2014) and was used in previous modelling studies (Burke et al., 2017; Koven et al., 2013). Observational studies traced isotopes within permafrost soils to analyze patterns and rates of carbon movement (Becher et al., 2013; Jelinski et al., 2017; Klaminder et al., 2014). They suggest the cryoturbation rate is not constant, and depends on climate and the characteristics of freeze-thaw cycles (Becher et al., 2013; Jelinski et al., 2017). Rates observed fall within the range 0.01-0.1 cm/year, but are uncertain due to a limited number of study sites. So far, every model that approximates cryoturbation including the UVic ESCM does so using a diffusive vertical mixing scheme adapted from the land surface model (LSM) ORCHIDEE (Koven et al., 2009), with K_v ranging from 5 to 15 cm^2/year (Burke et al., 2017; de Vrese et al., 2021; Koven et al., 2013). Given challenges in constraining K_v with observational data, we conduct a sensitivity analysis with K_v ranging from 1 to 10 cm^2/year to quantify the effect of the choice of K_V on permafrost carbon recovery. The chosen rate of 5 cm^2/year is the middle value within the sensitivity analysis, and is the same rate used by Burke et al. (2017) and Koven et al. (2013).

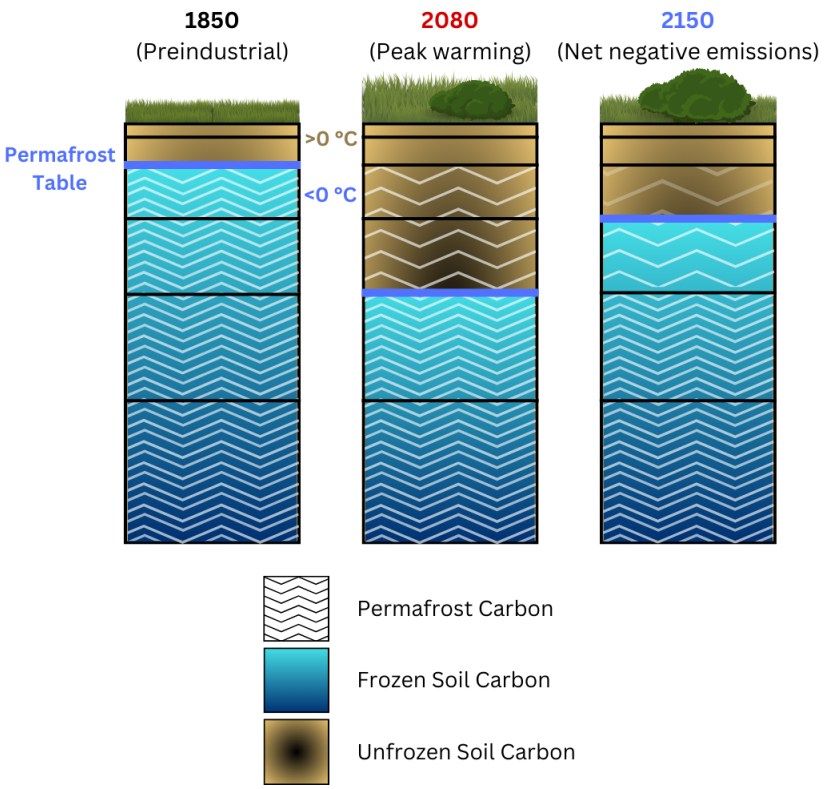

Figure 2 **Illustration of how the different soil carbon pool classes within the UVic ESCM evolve in a temperature overshoot scenario. Each column is a cross-sectional vertical representation of the six soil carbon layers and their classification at different stages of a temperature overshoot scenario. Soil carbon is reclassified as permafrost carbon when it diffuses through the permafrost table, and permafrost carbon can only be respired when a soil layer is above 0 °C. Therefore, the portion that is not respired remains classified as permafrost carbon despite the soil thawing in year 2080 and 2150. Frozen soil carbon represents permafrost soil carbon that is below 0 °C, and unavailable for respiration. The frozen carbon pool evolves as soil temperatures pass above and below 0°C in year 2080 and 2150. All frozen and unfrozen soil layers contain soil carbon.**

Figure 2 illustrates the different soil carbon pools in the permafrost region within the UVic ESCM. In permafrost grid cells, a separate permafrost carbon pool is created in addition to the regular soil carbon pool (MacDougall & Knutti, 2016). When soil carbon diffuses down from the active layer beyond the permafrost table into a frozen permafrost layer, it becomes part of the permafrost carbon pool. Carbon can only be added to the permafrost carbon pool through downward diffusion and can only be destroyed through microbial respiration when the permafrost soil layer thaws. Accordingly, permafrost carbon contained within a thawed soil layer is still considered part of the permafrost

carbon pool in the model unless it is respired. Since thawed soil layers are above 0°C, permafrost carbon in these layers can be respired over time unless the layer is refrozen. An additional model classification, the “sequestered frozen carbon pool”, exists in addition to the soil carbon and permafrost carbon pools. This pool tracks carbon in permafrost soil layers, that is, in soil frozen for more than two consecutive years following the standard definition of permafrost. Since all soil layers in the frozen carbon pool must be below 0°C, this pool represents carbon that cannot be respired into the atmosphere. The standard version of the model used here (2.10) only respires soil carbon as CO_2.

2.2. Experimental Design

First, the UVic ESCM is spun up to an equilibrium climate with preindustrial 1850 conditions, following the Coupled Model Intercomparison Project Phase 6 (CMIP6) protocol (Eyring et al., 2016). Forcings are set to constant 1850 values for CO_2 concentrations, non-CO_2 greenhouse gas (GHG) radiative forcing, aerosol optical depth, land use, and ozone. The volcanic forcing anomaly is set to its long-term mean, that is to the 1850-2014 average. The solar forcing is set to the mean of 1850-1873.

Next, a historical simulation is performed between 1850-2020 using transient forcing datasets based on observations (Eyring et al., 2016). Anthropogenic forcing data include CO_2 emissions derived from an observation-based CO_2 concentration estimate (Meinshausen et al., 2017), non-CO_2 GHGs, aerosols, land use, and ozone. Transient natural solar and volcanic forcings are also included. Forcing the model with CO_2 emissions allows for carbon cycle feedbacks to take place.

From 2020 to 2500 the model is forced with CO_2 emissions and non-CO_2 radiative forcings following Shared Socioeconomic Pathway (SSP) 1-2.6, an ambitious mitigation scenario that limits radiative forcing to 2.6 W/m^2 by the year 2100 (O’Neill et al., 2016). SSP1-2.6 is a scenario in which net negative emissions are achieved between years 2100-2140, and stabilizes to 2.0 W/m^2 beyond year 2200, with the long-term temperature likely to be below 1.5 °C (IPCC, 2021; O’Neill et al., 2016). The scenario was extended to year 2500 following Meinshausen et al. (2017). SSP1-2.6 and its extension serves as the high-mitigation, low overshoot reference scenario, which the idealized overshoot scenarios described below are based on.

A set of additional overshoot scenarios was designed to isolate the effect exerted by overshoot magnitude and duration (Figure 3a). Overshoot scenarios were designed by mimicking the bell-shaped curve of cumulative CO_2 emissions in SSP1-2.6, with each scenario reaching its peak SAT between years 2070-2075 (Figure 3c). A total of nine scenarios were created, systematically changing the overshoot magnitude and duration for each. Three different cumulative CO_2 emissions levels of 850, 1050, and 1250 GtC are held for 0, 30, or 60 years before gradually declining. The naming convention labels the maximum cumulative emissions (GtC), followed by a dash (-), and the duration (number of years) for which it was held. For instance, OS1050-0 reaches a maximum cumulative emission amount of 1050 GtC in 2075, which immediately starts to decline since this level is held for 0 years. Scenarios were designed to reach peak global average surface air temperatures that differ by 0.3°C. All scenarios eventually converge with the cumulative CO_2 emissions trajectory of SSP1-2.6. The convergence year depends on the overshoot duration, and occurs at 2150, 2190, or 2220 for 0, 30, or 60 years of peak emissions respectively. Cumulative CO_2 emissions for all scenarios are identical to SSP1-2.6 after convergence to allow for a direct comparison of long-term impacts. Idealized overshoot scenarios involve high levels of CDR that may not be feasible to achieve, but allow to explore a range of responses. CO_2 emissions from these scenarios were used to force the UVic ESCM.

Analysis focuses on OS1050-0, which follows a similar emissions trajectory as SSP5-3.4, which is a high overshoot marker scenario, with high emissions followed by rapid CO_2 removal (O'Neill et al., 2016). OS1050-0 is a slightly altered version of SSP5-3.4 to reach peak emissions at a similar time as SSP1-2.6, and for emissions to eventually merge together with SSP1-2.6 after the overshoot. Starting with the reference scenario OS1050-0, the effects of overshoot magnitude and duration on permafrost carbon variables are assessed for all scenarios. Figure 3a shows the emissions trajectories of all future scenarios.

Non-CO_2 GHG forcings in idealized overshoot scenarios are identical to SSP1-2.6 and its extension to year 2500 for all scenarios, and are described by Meinshausen et al. (2017, 2020). The same non-CO_2 GHG forcings are used to isolate and test only the impacts of CO_2 removal on permafrost carbon variables. Beyond year 2500, anthropogenic forcings are held constant at the 2500 levels. The volcanic forcing for

future simulations is set to the long-term mean, and solar forcings follow Matthes et al. (2017) until 2300, and the last solar cycle is repeated beyond 2300.

Chapter 3. Results

3.1. Atmospheric CO_2 & Temperature

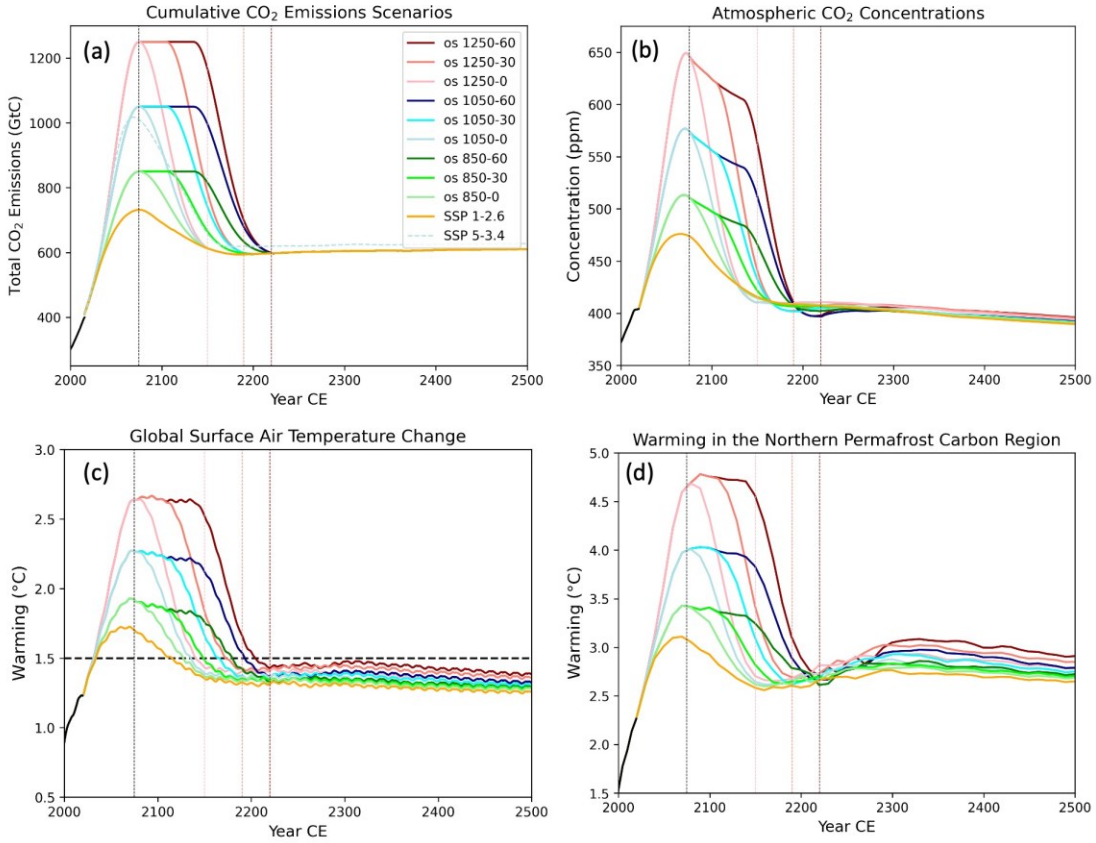

Figure 3 **Time series of a) cumulative CO_2 emissions for the scenarios used in this study, b) atmospheric CO_2 concentrations in response to emissions, c) global mean surface air temperature change since the 1850-1900 preindustrial mean, d) surface air temperature change averaged over grid cells that contain permafrost carbon. The black dotted vertical line at 2075 indicates the peak cumulative carbon emission year, and the coloured vertical lines indicate the years the OS scenario cumulative CO_2 emissions converge with those in SSP1-2.6: years 2150, 2190, and 2220 for scenarios with 0, 30 and 60 years overshoot duration, respectively.**

Anthropogenic CO_2 emissions (Figure 3a) used to drive the model have an immediate impact on atmospheric CO_2 concentrations (Figure 3b). By the time CO_2 emissions reach net zero, or cumulative emissions reach the peak or plateau in year 2075, concentrations have already started to decline for all scenarios. OS1050-0 CO_2 concentrations dip below the baseline SSP1-2.6 level before convergence at year ~2170

because of continued ocean carbon uptake after CO_2 emissions become net negative. The CO_2 concentration dip below the SSP1-2.6 level happens in all scenarios, and the dip is lower for longer overshoot durations.

Global mean SAT (Figure 3c) peaks or plateaus in 2075, the same year cumulative emissions peak or plateau for all OS scenarios, that is, CO_2 emissions reach net zero. Each 200 GtC of additional cumulative CO_2 emissions results in 0.35 °C of additional warming. SAT in OS1050-0 is slightly higher than in SSP1-2.6 during the zero-emissions phase after convergence of cumulative CO_2 emissions. A higher overshoot held for longer systematically leads to a slightly warmer temperature after convergence of cumulative emissions. In the high-overshoot long-duration scenario OS1250-60, the SAT is more than 0.1 °C warmer than the baseline at convergence in year 2220.

Mean SAT (Figure A1) within the northern high-latitude grid cells that contain permafrost carbon (Figure 3d) responds in a slightly different way compared to the global mean SAT. Warming in northern permafrost regions is approximately double the global average. Peak warming here in OS1050-0 is 4.0 °C as opposed to the global mean of 2.2 °C. A higher overshoot magnitude tends to delay the peak warming year: 2070 for all OS850 scenarios, 2080 for all OS1050 scenarios, and 2090 for OS1250-30 and OS1250-60. Additional high-latitude warming can be seen after CO_2 emissions reach zero in all scenarios. For 100 years after zero emissions are reached, permafrost region SAT slowly rises by ~0.2 °C in OS1050-0. After SAT initially converges following convergence of cumulative CO_2 emissions, SAT begins to spread between the different scenarios and fluctuates likely because of oscillations and restrengthening of the Atlantic Meridional Overturning Circulation (AMOC; Figure A2). SAT over the north Atlantic warms during the oscillation phase in OS1050-0 (Figure A1d), suggesting increased northward heat transport by the AMOC.

3.2. Permafrost Area

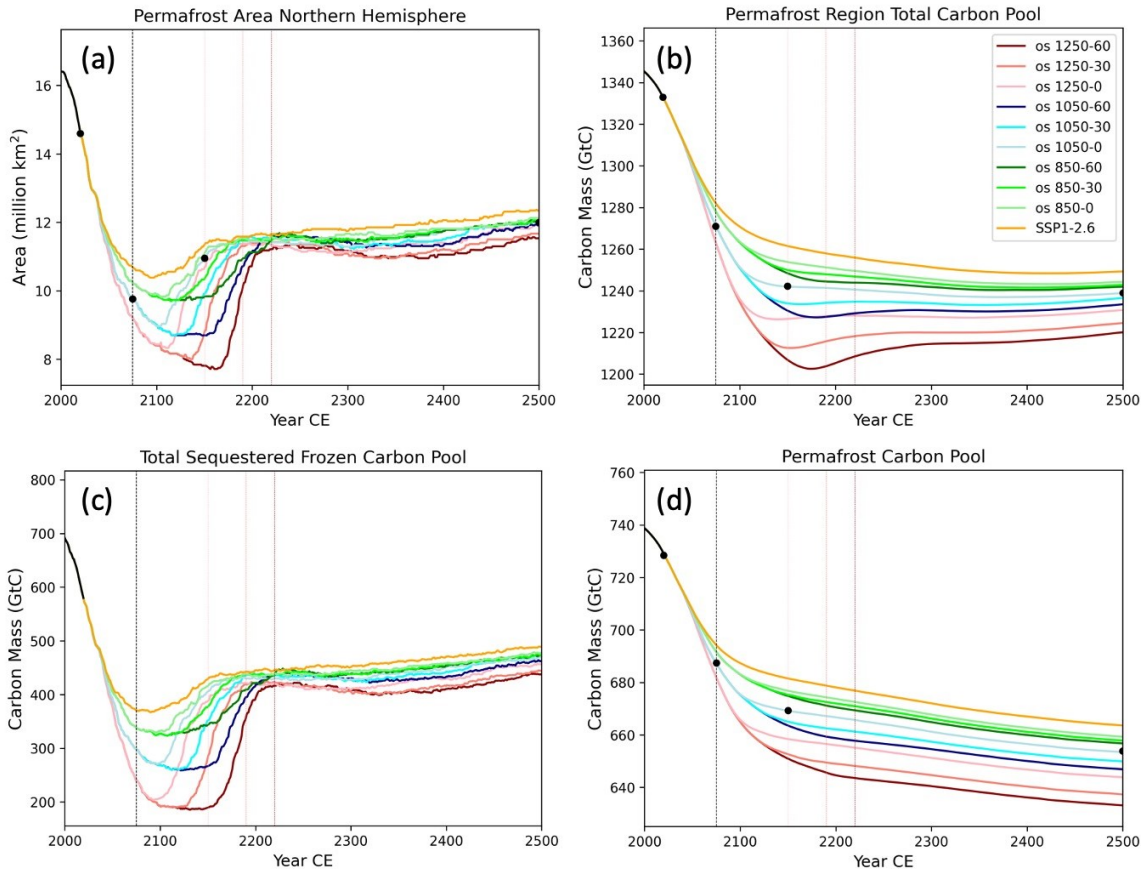

Figure 4 **Time series of a) total permafrost area in the northern hemisphere, b) total unfrozen and frozen soil carbon pool within the permafrost region, c) carbon contained only within frozen soils, d) permafrost carbon accumulated through the diffusion scheme. The dots indicate the year each spatial plot (Figures 4-6) represents in OS1050-0. The black dotted vertical line at 2075 indicates the peak cumulative carbon emission year, and the coloured vertical lines indicate the years the OS scenario cumulative CO_2 emissions converge with those in SSP1-2.6: years 2150, 2190, and 2220 for scenarios with 0, 30 and 60 years overshoot duration, respectively.**

Permafrost area in the northern hemisphere (Figure 4a) is sensitive to SAT changes, and declines in response to warming. Spatial plots show grid cells that contain at least one soil layer that has been frozen for more than two consecutive years, as per the definition of permafrost (Figure 5). Permafrost extent in 1850 (Figure 5a) covers most of the land surface north of 60 °N. Annual average soil temperatures are below 0 °C in all grid cells that contain permafrost (Figure A3a).

As the annual-mean soil temperature warms above 0 °C in response to SAT warming (Figure A3b), thaw begins at the southern extremities in 2020 (Figure 5b). Soil temperature warms relative to 1850 (Figure A4a) in all grid cells. By the time SAT reaches the peak in year 2080 for OS1050-0, more than 4 million km^2 of permafrost area is lost between years 2020 and 2080, which is over a quarter of the total area (Figure 4a/Figure 5b). Soil temperature continues to rise in all grid cells until peak warming, and temperature in a significant proportion of grid cells exceeds the melting point of water (0 °C) by 2080 (Figure A3c/Figure A4b). Despite global average SAT and soil temperature warming by more than 3 °C, Arctic soils north of 70 °N stay frozen at well below 0 °C.

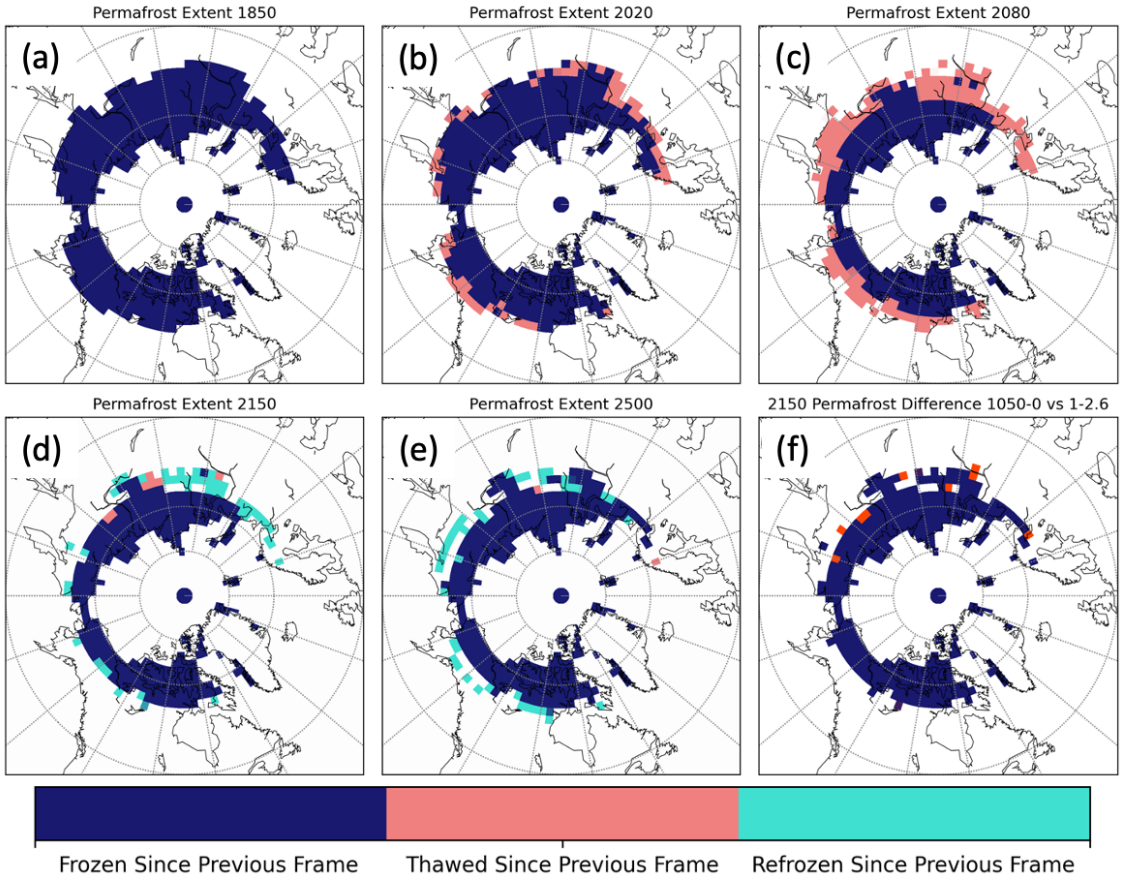

Figure 5 **Permafrost extent for OS1050-0 in year a) 1850, b) 2020, c) 2080, d) 2150, e) 2500. Dark blue grid cells have permafrost, and changes relative to the previous frame are given by light pink/blue colours. f) Differences in permafrost extent for OS1050-0 in year 2150 relative to the baseline SSP1-2.6. The red grid cells indicate the presence of permafrost in SSP1-2.6, but not in OS1050-0.**

Refreeze in OS1050-0 begins in 2110, approximately 30 years after global average SAT begins to cool (Figure 4a). After 2110, permafrost area increases rapidly.

By year 2150, there is substantial net gain of permafrost area relative to 2080, but there are still a few additional grid cells that have thawed (Figure 5d). Soil temperatures cool at roughly the same rate as they warmed during times of positive CO_2 emissions (Figure A4c), but the southern edges stay above 0 °C (Figure A3d).

Refreeze continues between the years 2150-2500, although two grid cells have lost permafrost during this period (Figure 5e). Permafrost region SAT is relatively stable by the year 2500, but is slightly warmer in 2500 compared to 2150 (Figure 3d/Figure A1d). In response, soil temperatures experience very little change after year 2150 (Figure A4d), with the southern edges staying close to 0 °C and the northern end staying well below 0 °C (Figure A3e).

Compared to the baseline SSP1-2.6, OS1050-0 shows very little difference in permafrost extent or soil temperature by the time emissions converge for the two scenarios in year 2150. Permafrost area recovers to a similar extent by 2150, with SSP1-2.6 having a slightly larger area (Figure 4a). The additional frozen grid cells in SSP1-2.6 are all at the southern edge of permafrost in Eurasia (Figure 5f). Soil temperatures are virtually identical for the two scenarios in the entire region (Figure A3f).

Change in permafrost area is sensitive to the magnitude and duration of overshoot (Figure 4a). A higher overshoot magnitude leads to more thaw, and the overshoot held for a longer period of time causes continuous thaw for the OS1250 scenarios. Minimum permafrost extent for OS850-0, 30, and 60 are identical, but extent continues to decrease when the peak temperature is held longer in OS1250. After a short time lag of about 3 decades relative to SAT cooling, refreeze begins in all scenarios. Total permafrost area converges to a similar level for the 9 OS scenarios approximately 3 decades after cumulative emissions converge with those in SSP1-2.6, but do not recover to the exact same extent. Shortly after convergence however, permafrost area diverges again between the different scenarios. This divergence behaviour mirrors Arctic SAT (Figure 3d), with a warmer temperature during the zero-emissions phase ultimately resulting in less permafrost area beyond year 2500.

3.3. Northern Permafrost Region Soil Carbon

The UVic ESCM approximates the natural system by distinguishing soil carbon within the permafrost region in three different pools as explained in section 2.1 and illustrated in Figure 2: permafrost region soil carbon pool, frozen carbon pool, and permafrost carbon pool. The permafrost region soil carbon pool (Figure 4b/Figure 6) includes all soil carbon within grid cells that have at least one soil layer containing permafrost carbon, including both soil and permafrost soil carbon pools. The frozen carbon pool (Figure 4c) includes carbon contained within frozen permafrost soils only, making it unavailable for respiration. The permafrost carbon pool (Figure 4d/Figure 7) is equivalent to “old carbon” and contains carbon that diffused down through the permafrost table during the UVic ESCM spin-up phase. While it is originally formed only in frozen layers, it includes carbon within frozen and thawed soil layers, which can be respired when the soil temperature is above 0 °C.

3.3.1. Spatial Patterns of Soil Carbon Loss and Gain

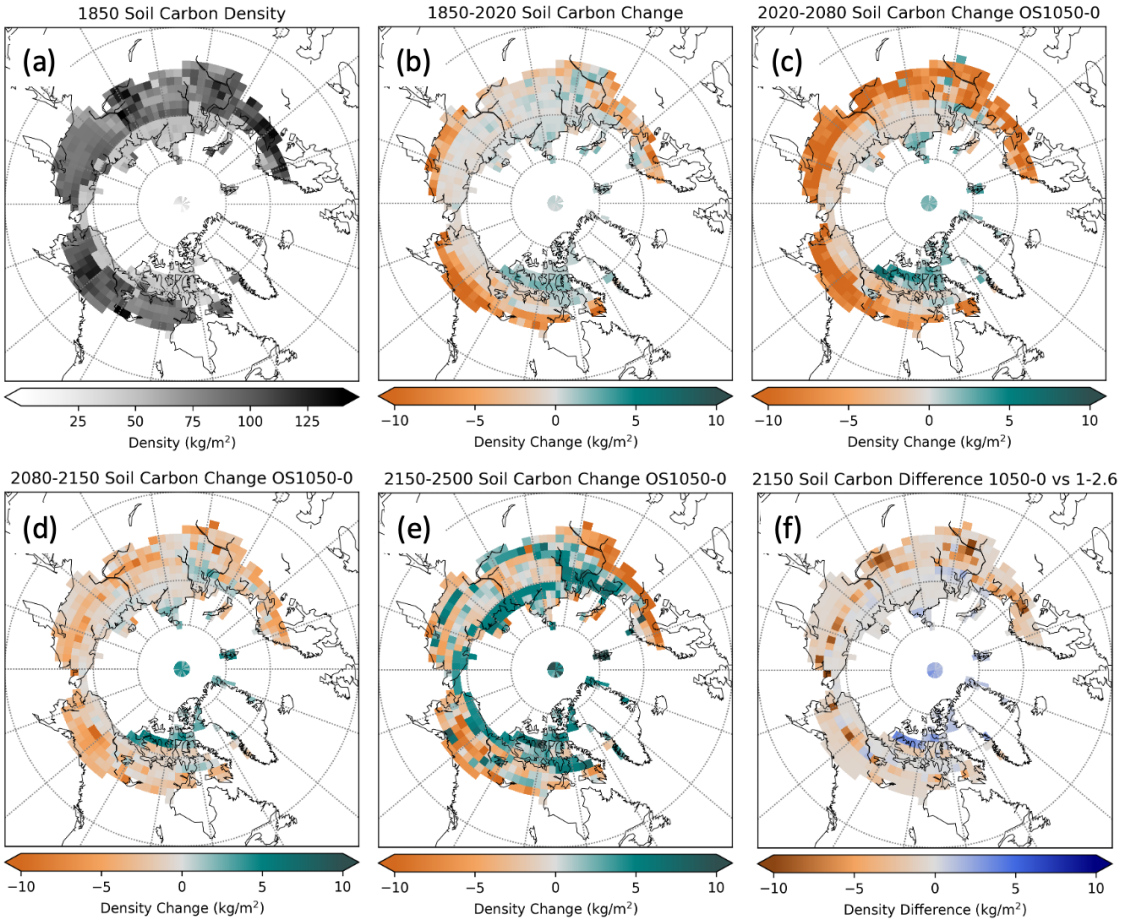

Figure 6 **Spatial distribution of a) permafrost region soil carbon density in 1850, b-e) soil carbon density change between 1850 and 2500. Each time-evolution panel shows the relative difference compared to the previous panel. f) soil carbon density difference between OS1050-0 and SSP1-2.6 in 2150. Spatial plots include all soil carbon, which is the sum of both the soil and permafrost carbon pools.**

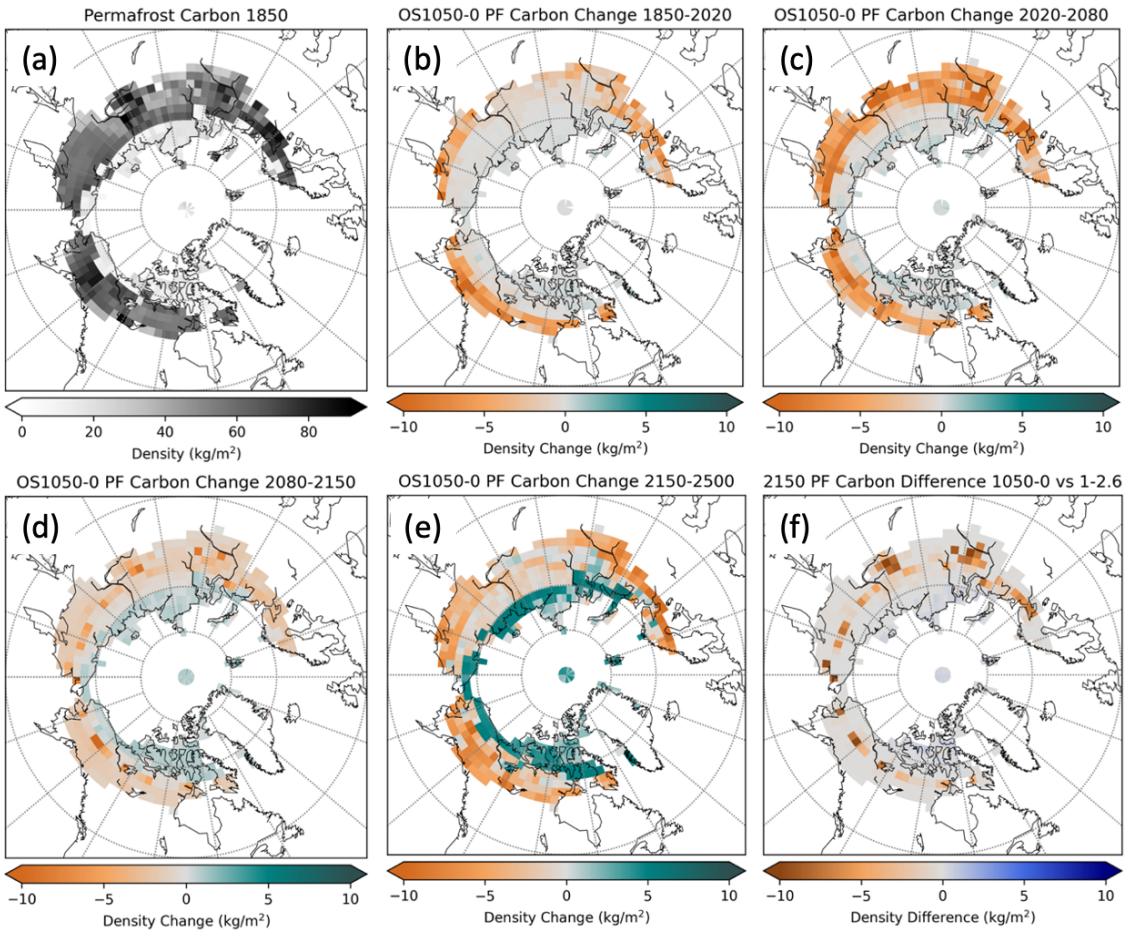

Figure 7 **Spatial distribution of a) permafrost carbon density in 1850, b-e) permafrost carbon density change between 1850 and 2500. Each time-evolution panel shows the relative difference compared to the previous panel. f) permafrost carbon density difference between OS1050-0 and SSP1-2.6 in 2150. Spatial plots show only the permafrost carbon pool, and do not include the soil carbon pool.**

The highest density of soil carbon within the northern high-latitude permafrost region can be found between 60-70 °N on continental north America and Eurasia (Figure 6a). The high-Arctic region north of 70 °N has a much lower density of soil carbon compared to the adjacent region in the south. Permafrost carbon is also distributed in the same way, and has high-density carbon-rich areas in central Alaska, central Russia, and along the Barents sea in western Europe (Figure 7a).

By 2020, carbon loss in both pools begins in the southern extremities of the permafrost region (Figure 6b/Figure 7b). Carbon loss accelerates and moves north between 2020-2080 (Figure 6c/Figure 7c), with the high-density grid cells (shown in Figure 6a/Figure 7a) losing particularly large amounts of carbon. The same regions also

experience the least amount of soil warming (Figure A4a/b). SAT (Figure A1a/b) warms globally during this period and soil temperature warms in the northern high latitudes, except for the grid cells where permafrost thaws. Soil temperature in grid cells at the northern edge of the region where permafrost carbon is lost stays at roughly the same soil temperature, at 0 °C (Figure A3b/c). A lack of warming here is likely because soils are thawing, with the warming contributing to latent heat of fusion instead of sensible heat. Minimal soil temperature warming in the discontinuous permafrost regions due to latent heat release has been confirmed by observations in the past decades (Biskaborn et al., 2019; Wang et al., 2023).

While the southern permafrost region loses large amounts of soil carbon during warming (1850-2080), the northern region starts to see a net gain in soil carbon (Figure 6b/c). Carbon gains are primarily north of 70 °N and farther south in some parts of Eurasia. The permafrost pool does not gain carbon during this time (Figure 7b/c). Despite the small gains in the north, carbon density declines at its most rapid rate from 2020-2080 in both the soil and permafrost carbon pools (Figure 4b/d). 60 GtC of total soil carbon is released to the atmosphere between 2020-2080 in OS1050-0, half of which is from the permafrost carbon pool.

During the SAT cooling phase (2080-2150), soil carbon still shows the same spatial pattern of losses and gains but in smaller magnitude (Figure 6d). Permafrost carbon loss in the south slows down significantly, while a net gain becomes apparent in the north (Figure 7d). Although global SAT reaches the end of the cooling phase in year 2150, soil temperatures stay close to or above 0 °C between latitudes 60-70°N (Figure A3d) and soil carbon continues to decline in this region. Averaged over the permafrost region, both the total soil and permafrost carbon pools decline rapidly beyond year 2080, but carbon loss slows down significantly by 2150 (Figure 4b/d). The permafrost region loses 19 GtC total soil carbon between 2080-2110, and 5 GtC total soil carbon between 2110-2150 in OS1050-0.

During the zero-emissions phase (2150-2500), soil carbon shows significant increases throughout the region north of 70 °N, but also in some regions farther south (Figure 6e). Soil and permafrost carbon gains are associated with vegetation changes, which is explained in section 3.3.2 below. Despite the latitudes 60-70 °N comprising a mix of soil carbon gains and losses, this latitude band predominantly experiences a net

carbon loss. The permafrost carbon pool also shows strong gains north of 70 °N, but almost no net gains anywhere further south (Figure 7e). Overall, the total permafrost region soil carbon pool stays close to neutral between 2150-2500 (Figure 4b), while the losses are still outweighing the gains in the permafrost carbon pool (Figure 4d). 15 GtC of total soil carbon is lost between latitudes 50-70 °N while 10 GtC is gained between 71-90 °N, whereas 23 GtC of permafrost carbon is lost in 50-70 °N and 8 GtC is gained 71-90 °N. Permafrost carbon recovery requires the additional process of vertical diffusive transport, making it slower to recover compared to the soil carbon pool.

3.3.2. High-Latitude Vegetation Changes

Soil and permafrost carbon gain in the northern high-latitude region in future scenarios originates from vegetation changes. As vegetation productivity increases in response to warming and increased CO_2 concentration due to the CO_2 fertilization effect, vegetation carbon density increases, which leads to more litterfall and soil carbon accumulation, and eventually adds to the permafrost carbon pool through diffusion.

As the land surface warms in the Arctic and the atmospheric CO_2 concentration increases, net primary productivity (NPP) increases (Figure A5) in the entire permafrost region during warming (1850-2080). As cooling begins and the CO_2 concentration decreases, NPP also declines (2080-2150). Between years 2150-2500, there are small NPP gains and losses depending on the region. Permafrost region NPP increases relative to the preindustrial mean (Figure A6a), since the year 2500 SAT in this region is ~3 °C warmer on average than preindustrial (Figure 3d).

Increased NPP contributes to vegetation carbon becoming denser in the northern high latitudes. Between 1850-2020, C3 grasses start to grow north of 70 °N, a region that was previously bare ground (Figure A7a). At the same time, shrubs are encroaching into regions previously covered primarily by C3 grass between 60-70 °N (Figure A7b). Shrubs continue to shift north between years 2020-2080 (Figure A7e), and begin to replace C3 grasses north of 70 °N by year 2150 (Figure A7h/k). Farther south, shrub density is decreasing in 60-70 °N where it was previously increasing. Shrubs are eventually replaced as coniferous trees encroach northwards after the year 2080 (Figure A7i/l). The ecosystem slowly evolves northward as warming continues, a phenomenon known as Arctic greening, transitioning from bare ground to grasslands, shrubs, and

conifers. Overall carbon density increases in the permafrost region, where vegetation growth was previously limited by cold temperatures.

The net flux of carbon into the soil is a balance between gains from vegetation litter and losses from soil respiration. The southern permafrost region losing soil carbon has a net negative soil carbon balance, while the northern region gaining carbon has a net positive balance (Figure A8b-e). Carbon originally contained in vegetation biomass makes its way into the soil through litterfall, with litterfall increasing as CO_2 concentration increases, SAT warms, and vegetation becomes more productive (Figure A6b). The spatial distribution of the net atmosphere-soil flux reveals that soil respiration dominates in the south (negative soil carbon flux), whereas increased litterfall dominates in the northern Arctic (positive soil carbon flux). The litterfall flux in the permafrost region evolves very similarly to NPP with a delay of a few years (Figure A6a/b), while the rate of soil respiration goes through a much larger increase and decrease in response to warming and cooling (Figure A6c). Overall, soil carbon losses substantially outweigh gains in the entire northern high-latitude region between years 1850-2350 (Figure A6d/Figure A8). After year 2350, the net soil flux becomes slightly positive for OS1050-0, resulting in accumulation of soil carbon in the permafrost region mostly north of 70 °N.

3.3.3. Soil Carbon Loss - Scenario Comparison and Long-Term Recovery

During the warming phase (1850-2080), carbon in previously frozen soil becomes available for respiration, causing the soil and permafrost carbon pools to decline along with the frozen carbon pool (Figure 4b-d). By year 2080, the soil carbon pools begin to diverge between the different overshoot scenarios; larger amounts of soil carbon are lost in scenarios with higher peak warming.

During the cooling phase (2080-2150), both the total soil and permafrost carbon pools continue to decline rapidly. After about year 2100, the frozen soil carbon pool begins to recover, which slows down soil and permafrost carbon losses in the peak-and-decline OS-0 scenarios. In the meantime, soil carbon continues to decline in the longer overshoot duration OS-30 and OS-60 scenarios, showing scenario divergence. By year 2150, it is clear that overshoot peak temperature determines how much soil carbon is initially lost, while warming held for longer causes continued carbon loss. A larger overshoot magnitude and longer overshoot duration combined exacerbate loss, with the

OS1250 scenarios showing further spread between the different durations compared to the OS850 scenarios.

Between 1850 and 2150, the total permafrost region soil carbon pool declines by 97 GtC in the lowest overshoot SSP1-2.6, while 152 GtC is lost in the highest overshoot OS1250-60. A majority of the losses are from the permafrost carbon pool, with 74 GtC and 104 GtC lost in SSP1-2.6 and OS1250-60 respectively, showing a spread of 30 GtC. A spatial comparison in year 2150 between SSP1-2.6 and OS1050-0 shows the scenario differences primarily in the middle of the permafrost region at ~65 °N (Figure 6f/Figure 7f), where soil temperatures always hover close to 0°C (Figure A3b-e).

After overshoot (2150-2500), the total permafrost region soil carbon pool becomes stable with minimal gains or losses. Soil carbon declines in SSP1-2.6 and the low-overshoot OS850 scenarios throughout this period, while carbon begins to accumulate in the high-overshoot OS1250 scenarios. Net soil carbon changes after year 2150 results from a balance between losses from respiration in the south, and gains from increased vegetation productivity and litterfall in the north. Soil carbon begins to accumulate earlier in scenarios with higher overshoot, but has lost a larger amount during warming. Between the years 2150 and 2500, 12 GtC of total soil carbon is lost in SSP1-2.6, while 14 GtC is gained in OS1250-60. Unlike the non-permafrost soil carbon pool, the permafrost carbon pool continues to decline in all scenarios at a consistent rate. 15-18 GtC of permafrost carbon is lost in each scenario between 2150 and 2500, still showing impacts of overshoot in year 2500. Similarly to SAT and total permafrost area, the frozen soil carbon pool recovers after year 2150 and converges to nearly the same level as the baseline after overshoot, showing that a large proportion of thawed soil carbon was not respired during the warming phase.

Between years 2500-3000, total permafrost region soil carbon increases for all scenarios (Figure A9a). After soil carbon diverges between scenarios during warming, they come closer to convergence throughout the millennium in the long term as soil carbon recovers more quickly in scenarios with larger losses during the warming phase. Enhanced vegetation productivity and increased vegetation in the high latitudes compensates for the larger soil carbon losses in the high overshoot scenarios, bringing the total carbon pool closer to the lower overshoot scenarios. Permafrost carbon increases slightly after year 2600 for all scenarios, accumulating at a constant rate as

carbon diffuses down into the permafrost pool (Figure A9c). Unlike the soil carbon pool however, permafrost carbon pools do not approach convergence between the scenarios at any point.

Long-term changes in permafrost region soil carbon (Figure A9a), frozen soil carbon (Figure A9b), and permafrost soil carbon (Figure A9c) show that high-latitude soil carbon loss is dependent on the magnitude and duration of overshoot. Warming impacts the soil carbon pool for at least several centuries, and total permafrost region soil carbon do not fully converge to the level in SSP1-2.6 in any scenario, despite cumulative CO_2 emissions being identical beyond year 2150. Results show that high-latitude soil carbon lost during overshoot is irreversible to the level in the baseline for at least multiple centuries.

3.4. Permafrost Carbon Recovery for Different Diffusion Rates

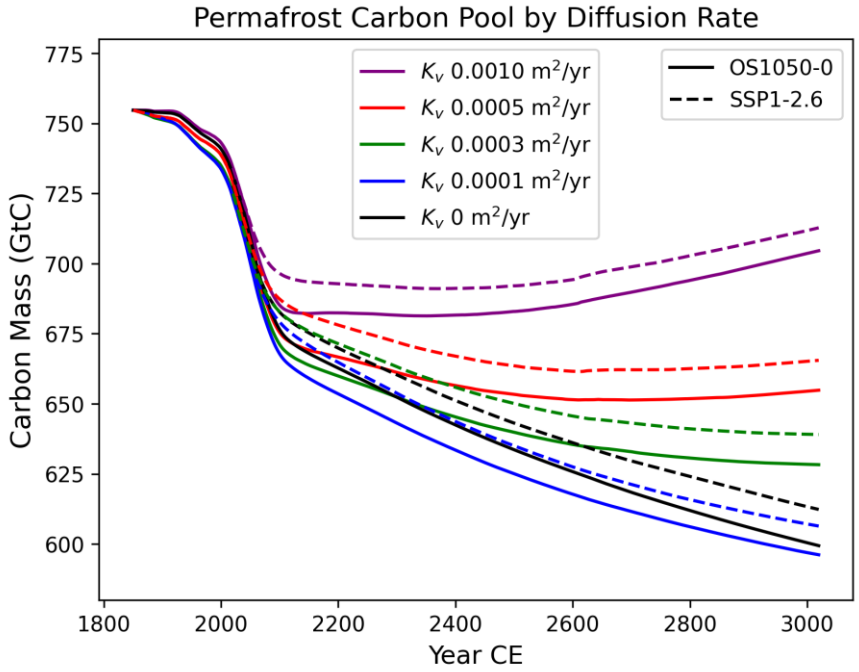

Figure 8 **Time series of the global permafrost carbon pool for the OS1050-0 and SSP1-2.6 scenarios using Kv diffusion rates between 0-0.001 m^2/year. Note that the time scale extends to the year 3000.**

Given that the diffusion parameter K_v (Equation 1, section 2.1) alters the rate of carbon accumulation in permafrost soils, the value chosen affects the timescale of

permafrost carbon recovery. To test the sensitivity of the results against the choice of the default K_v value 0.0005 m^2/year, this parameter was varied between 0 and 0.001 m^2/year, which reflects the range in the literature (Burke et al., 2017; de Vrese et al., 2021; Koven et al., 2009; Koven et al., 2013). The model was forced with the OS1050-0 and SSP1-2.6 scenarios to isolate the impact of the diffusion rate on the permafrost carbon pool.

Results of the comparison show that lower diffusion rates result in larger permafrost carbon losses and slower recovery, while higher diffusion rates lead to smaller losses and faster recovery (Figure 8). Initially, SAT warming in the permafrost region rapidly depletes permafrost carbon stocks at a similar rate until year 2080. Carbon loss slows down when warming is reversed after 2080 under all diffusion rates. After 2080, gradual loss continues for K_v 0-0.0005 m^2/year, but flattens out for K_v 0.001 m^2/year.

At the time of cumulative emissions convergence in year 2150, permafrost carbon amounts with K_v 0-0.0005 m^2/year are all lower in OS1050-0 than in SSP1-2.6. Altering the K_v value between 0-0.001 m^2/year changes the amount of permafrost carbon lost between 1850-2150, ranging from 73-96 GtC lost in OS1050-0 and 69-84 GtC in SSP1-2.6, showing a spread of 23-25 GtC between K_v values in each scenario. After year 2150, permafrost carbon pools continue to diverge between simulations with different diffusion rates. The spread in the permafrost carbon pool between the K_v values in year 2500 increases to 55-58 GtC for OS1050-0 and SSP1-2.6. Permafrost carbon amounts do not converge between OS1050-0 and SSP1-2.6 for any value of K_v beyond year 3000.

Permafrost carbon accumulation eventually overcomes losses with a K_v rate larger than 0.0005 m^2/year in both OS1050-0 and SSP1-2.6. Accumulation begins earlier for larger diffusion rates. For the largest value in the comparison (K_v 0.001 m^2/year), permafrost carbon begins to increase in the 2300s. For K_v 0.0005 m^2/year, permafrost carbon accumulates in the 2600s. In simulations with K_v values of 0.0001-0.0003 m^2/year, permafrost carbon continues to decline until year 3000. The total permafrost carbon pool has a spread of almost 100 GtC between the lowest and highest K_v values by year 3000.

3.5. Global Carbon Cycle Response

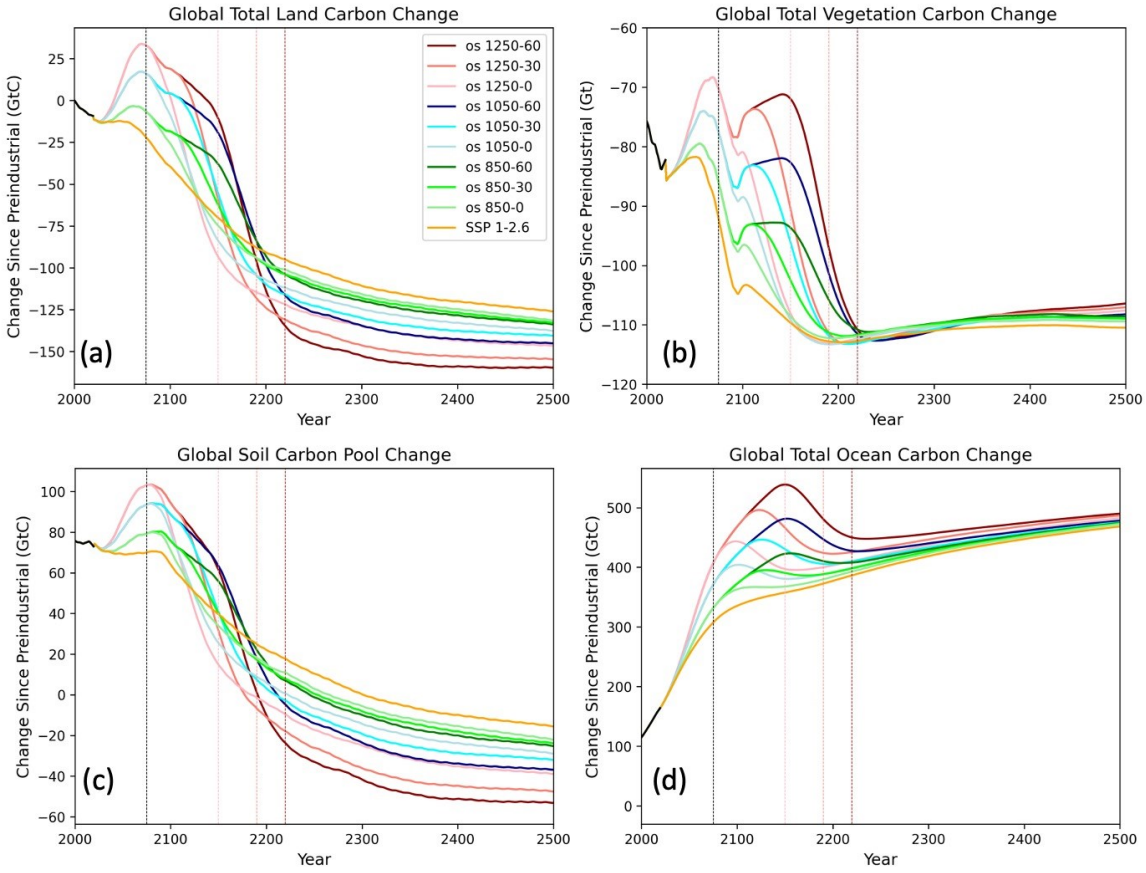

Figure 9 **Total global carbon pool for the a) land b) vegetation c) soil d) ocean. The black dotted vertical line at 2075 indicates the peak cumulative carbon emission year, and the coloured vertical lines indicate the years the OS scenario cumulative CO_2 emissions converge with those in SSP1-2.6: years 2150, 2190, and 2220 for scenarios with 0, 30 and 60 years overshoot duration, respectively.**

Positive and negative CO_2 emissions from anthropogenic and natural sources affect not only atmospheric CO_2 concentrations, but also the global land and ocean carbon cycle. Carbon released from permafrost region soils can freely interact with the atmosphere in emissions-driven simulations, but is not the only factor that impacts atmospheric CO_2 concentrations. The land and ocean can act as a carbon sink or source, mediating rapid changes in atmospheric CO_2.

The global land carbon pool is a carbon sink during the warming phase in all scenarios except for SSP1-2.6, but switches to a carbon source in all scenarios shortly before the peak warming year in 2075 (Figure 9a). A higher overshoot magnitude initially

leads to a larger amount of carbon stored on land, but the land carbon pool declines below the levels in the lower overshoot scenarios during the cooling phase between 2100-2150 in the OS-0 scenarios. By the time cumulative emissions converge for each overshoot duration in 2150, 2190, or 2220, the global land carbon pool is systematically smaller than the baseline SSP1-2.6 in scenarios with higher overshoot magnitudes.

A larger global land carbon pool during the warming phase is a result of more carbon stored in both vegetation (Figure 9b) and in the soil (Figure 9c). Global vegetation carbon rapidly responds to increasing and decreasing atmospheric CO_2 and temperature. Vegetation carbon amounts in each scenario converge with the level in SSP1-2.6 almost immediately after cumulative emissions converge, and slowly accumulates for all scenarios in the long term. The global soil carbon pool is slower to respond, but continuously declines after the cumulative emissions peak in a similar way to the total land carbon pool. After cumulative emissions convergence, both the global soil carbon pool and the global land carbon pool have a spread of ~40 GtC between SSP1-2.6 and the high overshoot magnitude, long-duration scenario OS1250-60. The 40 GtC spread between the baseline and the highest overshoot scenario is similar in quantity to the spread in permafrost carbon (30 GtC), and most of the differences between scenarios can be attributed to varying amounts of permafrost carbon respired during overshoot.

Following convergence of cumulative emissions for each overshoot duration (2150, 2190, or 2220), atmospheric CO_2 concentrations in all scenarios converge to nearly the same level as the baseline SSP1-2.6 (Figure 3a). Despite more permafrost soil carbon being released in scenarios with higher overshoot, differences do not show up in atmospheric CO_2 concentrations. The excess carbon lost from permafrost region soil is absorbed by the ocean.

The ocean acts as a carbon sink during warming, absorbing a large proportion of CO_2 emissions (Figure 9d). The ocean accumulates more carbon in scenarios with higher cumulative carbon emissions. In the OS-0 scenarios, the ocean continues to absorb carbon for ~25 years after peak warming in 2075, before outgassing some of the stored carbon back into the atmosphere. Larger amounts of ocean carbon are lost in scenarios with a higher magnitude of overshoot between 2100-2150, while ocean carbon uptake continues in SSP1-2.6. While peak warming is held in the OS-30 (2075-2105)

and OS-60 (2075-2135) scenarios, the ocean continues to absorb carbon, gradually reducing atmospheric CO_2 concentrations (Figure 3b). Following convergence of cumulative emissions, the ocean returns to being a carbon sink, gradually accumulating ocean carbon in the long term.

Chapter 4. Discussion

4.1. Implications of the Choice of Diffusion Rate for Permafrost Carbon Loss Reversibility

As shown in section 3.4., the response of the permafrost carbon pool to overshoot scenarios is sensitive to the K_v diffusion rate. A smaller K_v value leads to more permafrost carbon loss and slower recovery, and a larger value leads to a smaller amount lost and recovery within this millennium (Figure 8).

As atmospheric CO_2 concentrations increase and vegetation carbon uptake is enhanced by the CO_2 fertilization effect, a larger amount of carbon on the surface becomes available to be transported through the vertical layers. Land carbon changes at the northern high latitudes are especially sensitive to increased CO_2 and warming, which create more favourable conditions for plant growth (Figure A7). The additional carbon on the land surface eventually diffuses down through the soil layers, resulting in carbon accumulation in permafrost soils. The rate of permafrost carbon accumulation depends on the diffusion parameter K_v, with permafrost carbon recovering to a near-present (2020) level by the end of this millennium in the simulation with a K_v of 0.001 m^2/year, while recovering more slowly for simulations with lower K_v values.

Accurate projections of the timescale of permafrost carbon recovery will require better constraints on the value of K_v. Uncertainty in K_v could be reduced with more observational studies that span a wider geographical range. Regardless of the precise value of K_v, however, our study suggests that permafrost carbon loss is irreversible to the level in the SSP1-2.6 baseline for over a millennium.

4.2. Model Comparison

A limited number of modelling studies can be compared to the results from this study. De Vrese and Brovkin (2021) use a modified version of JSBACH, a land surface model (LSM) to analyze long-term Arctic change under simplified overshoot scenarios. The version of JSBACH used in their study uses a diffusion scheme to represent cryoturbation and a maximum vertical carbon diffusion rate of 0.0015 m^2/yr in permafrost soils, which decreases based on active later saturation and number of days soil

temperature crosses 0 °C (de Vrese et al., 2021). Schwinger et al. (2022) compare multiple overshoot scenarios with varying magnitudes and durations for 400 years using the Earth system model (ESM) NorESM2-LM. The Community Land Model (CLM5) that represents the terrestrial component of NorESM2 uses a maximum vertical carbon diffusion rate of 0.0005 m^2/yr in permafrost soils (Lawrence et al., 2019). Both models (modified JSBACH, and NorESM) include permafrost dynamics with multiple soil layers that include carbon. Cryoturbation is always represented by vertical diffusion adapted from the original scheme developed by Koven *et al.* (2009), which decreases with depth until a depth of 3m for the JSBACH and CLM5 (3.35m for the UVic ESCM).

When comparing the high-latitude soil carbon response to different overshoot scenarios with those in the UVic ESCM, all studies are in agreement. Carbon loss is scenario dependent, and impacts are proportional to the overshoot magnitude in the long-term for the UVic ESCM, JSBACH (de Vrese & Brovkin, 2021), and NorESM (Schwinger et al., 2022). Furthermore, the NorESM and UVic ESCM show continued loss when overshoot is held for a longer period of time. Decline is rapid during the warming phase, while continuous slow decline or minimal change is seen during the cooling phase.

While the JSBACH model shows a total high-latitude terrestrial carbon loss of ~30 GtC under 3 °C of warming, almost 100 GtC of combined high-latitude soil and vegetation carbon is lost in the OS1250-0 scenario in the UVic ESCM. The NorESM scenario with 3 °C of warming shows 40 GtC of permafrost region soil carbon loss and 60 GtC if peak warming is held for 100 years, while the UVic ESCM OS1250-0 scenario shows 130 GtC of carbon loss and 150 GtC for OS1250-60 (Figure A9c). There are substantial differences in the quantity of soil carbon loss between the UVic ESCM and the other two models. Differences can be attributed to the uncertain response of future climates and the terrestrial carbon cycle, especially in the northern high latitudes. Parameterizations, omitted processes, and uncertainties that contribute to model spread are discussed in the following section 4.3.1, including land-atmosphere CO_2 fluxes and feedback effects.

The UVic ESCM, JSBACH, and NorESM agree that high-latitude soil carbon loss is irreversible to a level that was present before overshoot for at least several centuries. Carbon stocks continue to decline for 500 years in the UVic, while the NorESM shows

no sign of recovery beyond the 400-year simulation. A more in-depth quantitative comparison of the high-latitude soil carbon loss is challenging due to the different overshoot scenarios used for each study. The UVic ESCM projects larger amounts of soil carbon loss relative to the modified JSBACH and NorESM, but the timeline for reversal is more than several centuries long in all three studies.

Overall, the high-latitude terrestrial carbon cycle responds similarly to temperature overshoot in LSMs and ESMs that include permafrost carbon processes. This includes the LSM JSBACH (de Vrese & Brovkin, 2021), and ESMs CESM2-WACCM (Melnikova et al., 2021) and NorESM2-LM (Schwinger et al., 2022). Like the UVic ESCM, all models listed above show a gradual gain of vegetation carbon at northern high-latitudes, known as Arctic greening. Changes in total land carbon at northern high-latitudes result from a balance between vegetation carbon increases from CO_2 fertilization and warming, and soil carbon losses from heterotrophic respiration (Schuur et al., 2022; Watts et al., 2021). While Arctic greening compensates for soil carbon loss in CESM2 under the SSP5-3.4 overshoot (Melnikova et al., 2021), soil carbon losses outweigh vegetation gains in the UVic ESCM, JSBACH (de Vrese & Brovkin, 2021), and NorESM (Schwinger et al., 2022) under a range of overshoot scenarios.

4.3. Limitations

4.3.1. Model Limitations

A major limitation of the UVic ESCM and most models that represent permafrost carbon is the use of a diffusive mixing scheme to approximate the process of cryoturbation. The scheme accurately represents the slow vertical movement of carbon, but may be overly sensitive to increased carbon density at the surface. High sensitivity is a drawback in scenarios with rapid changes in atmospheric CO_2 concentrations and terrestrial carbon stocks. So far, cryoturbation has only been represented by diffusion in LSMs and the land component of ESMs (Burke et al., 2017; de Vrese et al., 2021; Koven et al., 2013).

Another limitation of this study is the lack of representation of anaerobic methane (CH_4) respiration from soils. CH_4 release is an important process in permafrost regions,

and wetlands in particular are responsible for a large proportion of global CH_4 emissions (Saunois et al., 2020). A wetland methane emissions model is necessary to understand and quantify climate-CH_4 feedbacks (Nzotungicimpaye & Zickfeld, 2017), since natural CH_4 emissions are expected to cause additional warming this century (Schuur et al., 2022; Walter Anthony et al., 2018). Despite the high global warming potential of CH_4, a much larger proportion of gases will be released from permafrost thaw as CO_2, likely having a greater contribution to warming (Nzotungicimpaye & Zickfeld, 2017; Schädel et al., 2016). Nevertheless, a reliable quantification of carbon respired and emitted as both CH_4 and CO_2, as well as its feedback effects on the climate, is needed for accurate projections of carbon pool changes (A. Jones et al., 2018; Nzotungicimpaye & Zickfeld, 2017).

Abrupt thaw is another important process in permafrost regions not included in any ESM (IPCC, 2018, 2021). Abrupt thaw is an unpredictable small-scale process that changes the geomorphologic and hydrologic characteristics of landscapes through ground subsidence and thermokarst lake formation (Chartrand et al., 2023; de Vrese & Brovkin, 2021; Turetsky et al., 2020). It could release an additional 40% more carbon by 2300, as opposed to only gradual thaw represented in current models (Turetsky et al., 2020), primarily in the form of CH_4. Wildfires would also exacerbate abrupt thaw, which are not represented in ESMs either (Natali et al., 2021).

Models that include permafrost dynamics only consider near-surface soil carbon up to a depth of 3m (3.35m in the UVic ESCM; Schuur et al., 2022). A particular type of ice-rich and carbon-dense permafrost known as Yedoma deposits exist in deep soil beneath 3m (Schuur et al., 2022; Strauss et al., 2017). Yedoma deposits formed in unglaciated regions of Eurasia, Alaska, and Northwest Canada during the last glacial maximum (Strauss et al., 2017). Because of its high ice content, Yedoma deposits are susceptible to abrupt thaw, potentially causing strong feedbacks when the carbon is released into the atmosphere (Strauss et al., 2017). Deep permafrost areas outside of the Yedoma regions are poorly understood (Schuur et al., 2015).

Subsea permafrost is also omitted in models, which has been slowly thawing because of warm ocean water (Schuur et al., 2015). Carbon from subsea permafrost is being released from the East Siberian Arctic shelf, but catastrophic effects are unlikely because this carbon pool has been largely depleted by prior microbial decomposition

(Mishra et al., 2013; Shakhova et al., 2015). Nevertheless, subsea permafrost thaw is an uncertain process that cannot be ignored.

Land carbon cycle processes and their response to future climate change are highly uncertain. Present-day land carbon pools and flux data are collected in different regions around the globe, and modelled at coarse resolutions to provide global estimates (Jian et al., 2018; Varney et al., 2022; Warner et al., 2019). Soil respiration, NPP, and litterfall rates can be estimated based on observational data, but responses to future climate change remains a large source of uncertainty (Arora et al., 2020). The northern high latitudes are especially prone to changes in the future, with Arctic greening expected to alter ecosystem carbon distribution as well as respiration rates and NPP (Mekonnen et al., 2021). Carbon cycle feedbacks impact vegetation and land carbon pools, and the strength of the CO_2 fertilization effect is a particularly large source of uncertainty (Arora et al., 2013, 2020). Due to the combined uncertainties, ESMs do not agree on whether the terrestrial biosphere will be a carbon source or sink by the end of the century (Arora et al., 2013; Friedlingstein et al., 2014; Qiu et al., 2023). Fluxes and feedbacks between the atmosphere and land contribute to changes in the soil and vegetation carbon pools, and the uncertainties associated with each component ultimately affect the rate of permafrost region carbon loss and accumulation.

Many recent ESMs represent nutrient cycles, which are not included in the UVic ESCM. Nutrients such as nitrogen and phosphorus affect vegetation dynamics especially in the northern high latitudes (C. D. Koven et al., 2015; Mekonnen et al., 2021). Permafrost thaw releases nitrogen which enhances vegetation productivity, but future changes in the nitrogen cycle remain highly uncertain (C. D. Koven et al., 2015; Mekonnen et al., 2018). Vegetation in Tundra ecosystems is constantly competing for light, water, and nutrients, but plant functional types (PFTs; groups of plant species that share similar characteristics and environmental responses) and competition between them are highly parameterized in models (Mekonnen et al., 2021). The UVic ESCM has a total of 5 PFTs, of which only 2 are present in the permafrost region. An accurate prediction of Arctic greening is not possible without fully accounting for nutrients and vegetation dynamics.

Thermal properties of soil are influenced by insulation from soil organic matter (SOM) and snow. SOM acts as a thermal insulator, which alters the characteristics of

permafrost thaw (C. D. Koven et al., 2009b; Zhu et al., 2019). SOM content also alters the hydrological properties of soil, impacting evapotranspiration rates (de Vrese & Brovkin, 2021). Snow also insulates the soil beneath, altering the surface energy balance (Wang et al., 2023). The UVic ESCM includes the thermal effects of snow, but is highly parameterized. Insulation from SOM is not represented in the UVic ESCM. Uncertainties regarding soil temperature and moisture content contribute to uncertainty in soil respiration rates, and ultimately the total soil carbon pool.

4.3.2. Scenario Limitations

The scenarios designed for this study are idealized to allow for systematic comparison of the effects of overshoot magnitude and duration. Emission rates are realistic based on historical and expected socioeconomic development, but the CDR rate is high for OS1250 which peaks at net negative emissions of 14 GtC/yr, and 9 GtC/yr in 2100 for OS1050, which is similar to SSP5-3.4. For reference, SSP1-2.6 will require a CO_2 removal rate of approximately 5 GtC/yr in 2100 (Brazzola et al., 2021), with a cumulative total removal of more than 200 GtC between 2010-2100 (Riahi et al., 2017). CDR technologies currently exist on a small scale, and need to be drastically improved and scaled up to make these scenarios possible (IPCC, 2023; C. D. Jones et al., 2016; P. Smith et al., 2016).

A simplification of the emissions design is that non-CO_2 forcings follow SSP1-2.6 for all scenarios, whereas in reality, they should increase or decrease consistently with the prescribed CO_2 emissions. The purpose of the simplification is to isolate the effects of overshoot magnitude and duration by altering only CO_2 emissions, without the confounding effects of non-CO_2 forcings.

4.4. Implications of High-latitude Carbon Release

Northern permafrost region soil carbon loss contributes to additional emissions on top of fossil fuel emissions and warming through a positive feedback. Further warming from carbon cycle feedbacks despite a reduction in anthropogenic emissions could lead to a failure to meet the intended temperature goals. While the results show that ocean carbon uptake compensates for permafrost carbon release and prevents atmospheric CO_2 from rising, there are uncertainties within many of the represented

processes. Permafrost region carbon loss could require further emissions reductions to meet policy goals, especially if larger amounts are rapidly released.

Limiting warming to 1.5 and 2 °C above preindustrial levels requires an accurate estimation of allowable emissions, also known as the remaining carbon budget. Dependency of high-latitude soil carbon loss on overshoot characteristics implies that the carbon budget is nonlinear and path dependent (Gasser et al., 2018). Results of the present study show that overshoot magnitude and duration have long-term impacts on high-latitude carbon release. Since most ESMs do not account for permafrost carbon emissions, carbon budget calculations that rely on simulations with these models are uncertain and will likely need to be further reduced (Natali et al., 2021).

The UVic ESCM shows a variable amount of permafrost carbon release depending on the K_v diffusion rate, ranging from 73-96 GtC lost between 1850-2150 in OS1050-0 (Figure 8). Permafrost carbon is more sensitive to warming in the UVic ESCM compared to other models (modified JSBACH and NorESM), but the projected carbon release is significant despite the possible overestimate. Put into perspective, the remaining carbon budget from year 2023 for a 50% chance of staying below 1.5 °C of warming is about 70 GtC (Forster et al., 2023). While the goal here is not to quantify the permafrost carbon feedback, models that include permafrost carbon show the potential for significant contribution to warming over time.

An improved understanding of the permafrost carbon feedback and sensitivity of permafrost carbon loss to warming will reduce carbon budget uncertainties, and ultimately help inform policy decisions. Regardless of the uncertainties, immediate reductions in emissions combined with CO_2 removals is necessary to achieve the climate goals of the Paris Agreement.

Chapter 5. Conclusions

Results of this study show that northern high-latitude soil carbon is lost rapidly during warming due to permafrost thaw. Despite permafrost partly refreezing during the cooling phase of overshoot, permafrost carbon loss continues. Soil carbon loss is path dependent, and both a higher magnitude and longer duration of temperature overshoot causes more loss. After cumulative emissions in overshoot scenarios converge with the baseline scenario SSP1-2.6, Arctic temperature and permafrost extent recover near the level in the baseline scenario, whereas the soil carbon pool does not. Differences in the high latitude soil and permafrost carbon pool persist for more than several centuries. Changes induced during temperature overshoot leaves a legacy in the Arctic carbon cycle, and are irreversible for at least several centuries.

Continuous permafrost carbon loss could contribute to additional warming through a positive feedback on the climate, even if anthropogenic greenhouse gas emissions reach net zero. Despite the potential emissions from thaw, the permafrost carbon feedback is currently not fully incorporated in allowable emissions estimates to meet temperature targets. As a consequence, continued permafrost carbon loss after overshoot could mean a failure to meet the Paris Agreement temperature goals, unless additional emissions are balanced by removals. There are many uncertainties regarding permafrost carbon release, and further constraints of relevant processes and more accurate quantification is necessary to assess its contribution to warming.

Long-term continuous emissions from the high-latitude carbon pool accentuates the importance of immediate mitigation. Scenario dependence and irreversibility of permafrost carbon loss creates the need to limit the amount and duration of overshoot through ambitious emission cuts to minimize carbon losses from permafrost soils.

Future research should include model development to improve accuracy in the representation of permafrost carbon processes. Expanding soil carbon modules to include vertical layers and permafrost dynamics in more LSMs and ESMs, and an improved representation of cryoturbation processes will help fully represent the terrestrial carbon cycle. Constraining CO_2 fertilization (Hajima et al., 2014; McGuire et al., 2016), NPP sensitivity (McGuire et al., 2018), and having better vegetation dynamics to simulate Arctic greening (Miner et al., 2022) will help reduce uncertainty. Wetland

methane emissions models can be developed further and improved based on observed emissions using remote sensing (Miner et al., 2022). Wetland CH_4 emissions can be integrated into ESMs to project CH_4 emissions in addition to CO_2 emissions in response to warming (Nzotungicimpaye et al., 2021). Observational data including surface CO_2/CH_4 fluxes and biomass estimates especially in the remote areas of the Arctic will help validate and improve models (Mavrovic et al., 2023; Miner et al., 2022).

Model intercomparisons and ensembles will help produce more robust results. An intercomparison will require having standardized simulation designs with potential future CO_2 emissions and concentrations to directly compare outputs. With temperature overshoot fast becoming inevitable to reach the 1.5 °C and 2 °C targets, running model simulations with a larger set of overshoot scenarios in addition to SSP1-2.6 and SSP5-3.4 would help to understand Earth system responses. In addition to CESM and NorESM, more fully coupled ESMs will need to have a permafrost carbon representation to allow for a fair comparison of results. Ultimately, a model ensemble constrained by observations will provide the most likely range of the future permafrost carbon response.

References

Arora, V. K., Boer, G. J., Friedlingstein, P., Eby, M., Jones, C. D., Christian, J. R., Bonan, G., Bopp, L., Brovkin, V., Cadule, P., Hajima, T., Ilyina, T., Lindsay, K., Tjiputra, J. F., & Wu, T. (2013). Carbon–Concentration and Carbon–Climate Feedbacks in CMIP5 Earth System Models. *Journal of Climate*, *26*(15), 5289–5314. https://doi.org/10.1175/JCLI-D-12-00494.1

Arora, V. K., Katavouta, A., Williams, R. G., Jones, C. D., Brovkin, V., Friedlingstein, P., Schwinger, J., Bopp, L., Boucher, O., Cadule, P., Chamberlain, M. A., Christian, J. R., Delire, C., Fisher, R. A., Hajima, T., Ilyina, T., Joetzjer, E., Kawamiya, M., Koven, C. D., … Ziehn, T. (2020). Carbon–concentration and carbon–climate feedbacks in CMIP6 models and their comparison to CMIP5 models. *Biogeosciences*, *17*(16), 4173–4222. https://doi.org/10.5194/bg-17-4173-2020

Avis, C. A. (2012). *Simulating the present-day and future distribution of permafrost in the UVic Earth System Climate Model* [Thesis]. https://dspace.library.uvic.ca/handle/1828/4030

Avis, C. A., Weaver, A. J., & Meissner, K. J. (2011). Reduction in areal extent of high-latitude wetlands in response to permafrost thaw. *Nature Geoscience*, *4*(7), Article 7. https://doi.org/10.1038/ngeo1160

Becher, M., Olid, C., & Klaminder, J. (2013). Buried soil organic inclusions in non-sorted circles fields in northern Sweden: Age and Paleoclimatic context. *Journal of Geophysical Research: Biogeosciences*, *118*(1), 104–111. https://doi.org/10.1002/jgrg.20016

Biskaborn, B. K., Smith, S. L., Noetzli, J., Matthes, H., Vieira, G., Streletskiy, D. A., Schoeneich, P., Romanovsky, V. E., Lewkowicz, A. G., Abramov, A., Allard, M., Boike, J., Cable, W. L., Christiansen, H. H., Delaloye, R., Diekmann, B., Drozdov, D., Etzelmüller, B., Grosse, G., … Lantuit, H. (2019). Permafrost is warming at a global scale. *Nature Communications*, *10*(1), Article 1. https://doi.org/10.1038/s41467-018-08240-4

Bitz, C. M., & Lipscomb, W. H. (1999). An energy-conserving thermodynamic model of sea ice. *Journal of Geophysical Research: Oceans*, *104*(C7), 15669–15677. https://doi.org/10.1029/1999JC900100

Bockheim, J. G. (2007). Importance of Cryoturbation in Redistributing Organic Carbon in Permafrost-Affected Soils. *Soil Science Society of America Journal*, *71*(4), 1335–1342. https://doi.org/10.2136/sssaj2006.0414N

Boucher, O., Halloran, P. R., Burke, E. J., Doutriaux-Boucher, M., Jones, C. D., Lowe, J., Ringer, M. A., Robertson, E., & Wu, P. (2012). Reversibility in an Earth System model in response to CO_2 concentration changes. *Environmental Research Letters*, *7*(2), 024013. https://doi.org/10.1088/1748-9326/7/2/024013

Brazzola, N., Wohland, J., & Patt, A. (2021). Offsetting unabated agricultural emissions with CO2 removal to achieve ambitious climate targets. *PLOS ONE*, *16*(3), e0247887. https://doi.org/10.1371/journal.pone.0247887

Burke, E. J., Chadburn, S. E., & Ekici, A. (2017). A vertical representation of soil carbon in the JULES land surface scheme (vn4.3_permafrost) with a focus on permafrost regions. *Geoscientific Model Development*, *10*(2), 959–975. https://doi.org/10.5194/gmd-10-959-2017

Burke, E. J., Chadburn, S. E., Huntingford, C., & Jones, C. D. (2018). CO2 loss by permafrost thawing implies additional emissions reductions to limit warming to 1.5 or 2 °C. *Environmental Research Letters*, *13*(2), 024024. https://doi.org/10.1088/1748-9326/aaa138

Chartrand, S. M., Jellinek, A. M., Kukko, A., Galofre, A. G., Osinski, G. R., & Hibbard, S. (2023). High Arctic channel incision modulated by climate change and the emergence of polygonal ground. *Nature Communications*, *14*(1), Article 1. https://doi.org/10.1038/s41467-023-40795-9

Cox, P. (2001). *Description of the "TRIFFID" Dynamic Global Vegetation Model*.

de Vrese, P., & Brovkin, V. (2021). Timescales of the permafrost carbon cycle and legacy effects of temperature overshoot scenarios. *Nature Communications*, *12*(1), 2688. https://doi.org/10.1038/s41467-021-23010-5

de Vrese, P., Stacke, T., Kleinen, T., & Brovkin, V. (2021). Diverging responses of high-latitude CO2 and CH4 emissions in idealized climate change scenarios. *The Cryosphere*, *15*(2), 1097–1130. https://doi.org/10.5194/tc-15-1097-2021

Ehlert, D., & Zickfeld, K. (2018). Irreversible ocean thermal expansion under carbon dioxide removal. *Earth System Dynamics*, *9*(1), 197–210. https://doi.org/10.5194/esd-9-197-2018

Eliseev, A. V., Demchenko, P. F., Arzhanov, M. M., & Mokhov, I. I. (2014). Transient hysteresis of near-surface permafrost response to external forcing. *Climate Dynamics*, *42*(5), 1203–1215. https://doi.org/10.1007/s00382-013-1672-5

Eyring, V., Bony, S., Meehl, G. A., Senior, C. A., Stevens, B., Stouffer, R. J., & Taylor, K. E. (2016). Overview of the Coupled Model Intercomparison Project Phase 6 (CMIP6) experimental design and organization. *Geoscientific Model Development*, *9*(5), 1937–1958. https://doi.org/10.5194/gmd-9-1937-2016

Fanning, A. F., & Weaver, A. J. (1996). An atmospheric energy-moisture balance model: Climatology, interpentadal climate change, and coupling to an ocean general circulation model. *Journal of Geophysical Research: Atmospheres*, *101*(D10), 15111–15128. https://doi.org/10.1029/96JD01017

Forster, P. M., Smith, C. J., Walsh, T., Lamb, W. F., Lamboll, R., Hauser, M., Ribes, A., Rosen, D., Gillett, N., Palmer, M. D., Rogelj, J., von Schuckmann, K., Seneviratne, S. I., Trewin, B., Zhang, X., Allen, M., Andrew, R., Birt, A., Borger, A., … Zhai, P. (2023). Indicators of Global Climate Change 2022: Annual update of large-scale indicators of the state of the climate system and human influence. *Earth System Science Data*, *15*(6), 2295–2327. https://doi.org/10.5194/essd-15-2295-2023

Friedlingstein, P., Meinshausen, M., Arora, V. K., Jones, C. D., Anav, A., Liddicoat, S. K., & Knutti, R. (2014). Uncertainties in CMIP5 Climate Projections due to Carbon Cycle Feedbacks. *Journal of Climate*, *27*(2), 511–526. https://doi.org/10.1175/JCLI-D-12-00579.1

Gasser, T., Kechiar, M., Ciais, P., Burke, E. J., Kleinen, T., Zhu, D., Huang, Y., Ekici, A., & Obersteiner, M. (2018). Path-dependent reductions in CO2 emission budgets caused by permafrost carbon release. *Nature Geoscience*, *11*(11), 830–835. https://doi.org/10.1038/s41561-018-0227-0

Hajima, T., Kawamiya, M., Watanabe, M., Kato, E., Tachiiri, K., Sugiyama, M., Watanabe, S., Okajima, H., & Ito, A. (2014). Modeling in Earth system science up to and beyond IPCC AR5. *Progress in Earth and Planetary Science*, *1*(1), 29. https://doi.org/10.1186/s40645-014-0029-y

IPCC. (2018). *An IPCC Special Report on the impacts of global warming of 1.5°C above pre-industrial levels and related global greenhouse gas emission pathways, in the context of strengthening the global response to the threat of climate change, sustainable development, and efforts to eradicate poverty*.

IPCC. (2021). *Climate Change 2021: The Physical Science Basis. Contribution of Working Group I to the Sixth Assessment Report of the Intergovernmental Panel on Climate Change*. Cambridge University Press.

IPCC. (2023). *Climate Change 2023: Synthesis Report. Contribution of Working Groups I, II and III to the Sixth Assessment Report of the Intergovernmental Panel on Climate Change [Core Writing Team, H. Lee and J. Romero (eds.)]*. IPCC, Geneva, Switzerland.

Jackson, L. C., & Wood, R. A. (2018). Hysteresis and Resilience of the AMOC in an Eddy-Permitting GCM. *Geophysical Research Letters*, *45*(16), 8547–8556. https://doi.org/10.1029/2018GL078104

Jelinski, N. A., Yoo, K., & Klaminder, J. (2017). Utilising a Suite of Isotopic and Elemental Tracers to Constrain Cryoturbation Rates and Patterns in a Non-sorted Circle. *Permafrost and Periglacial Processes*, *28*(4), 634–648. https://doi.org/10.1002/ppp.1944

Jian, J., Steele, M. K., Thomas, R. Q., Day, S. D., & Hodges, S. C. (2018). Constraining estimates of global soil respiration by quantifying sources of variability. *Global Change Biology*, *24*(9), 4143–4159. https://doi.org/10.1111/gcb.14301

Jones, A., Haywood, J. M., & Jones, C. D. (2018). Can reducing black carbon and methane below RCP2.6 levels keep global warming below 1.5 °C? *Atmospheric Science Letters*, *19*(6), e821. https://doi.org/10.1002/asl.821

Jones, C. D., Ciais, P., Davis, S. J., Friedlingstein, P., Gasser, T., Peters, G. P., Rogelj, J., van Vuuren, D. P., Canadell, J. G., Cowie, A., Jackson, R. B., Jonas, M., Kriegler, E., Littleton, E., Lowe, J. A., Milne, J., Shrestha, G., Smith, P., Torvanger, A., & Wiltshire, A. (2016). Simulating the Earth system response to negative emissions. *Environmental Research Letters*, *11*(9), 095012. https://doi.org/10.1088/1748-9326/11/9/095012

Klaminder, J., Yoo, K., Olid, C., Ramebäck, H., & Vesterlund, A. (2014). Using Short-lived Radionuclides to Estimate Rates of Soil Motion in Frost Boils. *Permafrost and Periglacial Processes*, *25*(3), 184–193. https://doi.org/10.1002/ppp.1811

Koven, C. D., Friedlingstein, P., Ciais, P., Khvorostyanov, D., Krinner, G., & Tarnocai, C. (2009). On the formation of high-latitude soil carbon stocks: Effects of cryoturbation and insulation by organic matter in a land surface model. *Geophysical Research Letters*, *36*(21). https://doi.org/10.1029/2009GL040150

Koven, C. D., Riley, W. J., Subin, Z. M., Tang, J. Y., Torn, M. S., Collins, W. D., Bonan, G. B., Lawrence, D. M., & Swenson, S. C. (2013). The effect of vertically resolved soil biogeochemistry and alternate soil C and N models on C dynamics of CLM4. *Biogeosciences*, *10*(11), 7109–7131. https://doi.org/10.5194/bg-10-7109-2013

Koven, C. D., Schuur, E. a. G., Schädel, C., Bohn, T. J., Burke, E. J., Chen, G., Chen, X., Ciais, P., Grosse, G., Harden, J. W., Hayes, D. J., Hugelius, G., Jafarov, E. E., Krinner, G., Kuhry, P., Lawrence, D. M., MacDougall, A. H., Marchenko, S. S., McGuire, A. D., … Turetsky, M. (2015). A simplified, data-constrained approach to estimate the permafrost carbon–climate feedback. *Philosophical Transactions of the Royal Society A: Mathematical, Physical and Engineering Sciences*, *373*(2054), 20140423. https://doi.org/10.1098/rsta.2014.0423

Koven, C., Friedlingstein, P., Ciais, P., Khvorostyanov, D., Krinner, G., & Tarnocai, C. (2009). On the formation of high-latitude soil carbon stocks: Effects of cryoturbation and insulation by organic matter in a land surface model. *Geophysical Research Letters*, *36*(21). https://doi.org/10.1029/2009GL040150

Lawrence, D. M., Fisher, R. A., Koven, C. D., Oleson, K. W., Swenson, S. C., Bonan, G., Collier, N., Ghimire, B., van Kampenhout, L., Kennedy, D., Kluzek, E., Lawrence, P. J., Li, F., Li, H., Lombardozzi, D., Riley, W. J., Sacks, W. J., Shi, M., Vertenstein, M., … Zeng, X. (2019). The Community Land Model Version 5: Description of New Features, Benchmarking, and Impact of Forcing Uncertainty. *Journal of Advances in Modeling Earth Systems*, *11*(12), 4245–4287. https://doi.org/10.1029/2018MS001583

Li, X., Zickfeld, K., Mathesius, S., Kohfeld, K., & Matthews, J. B. R. (2020). Irreversibility of Marine Climate Change Impacts Under Carbon Dioxide Removal. *Geophysical Research Letters*, *47*(17), e2020GL088507. https://doi.org/10.1029/2020GL088507

MacDougall, A. H., Avis, C. A., & Weaver, A. J. (2012). Significant contribution to climate warming from the permafrost carbon feedback. *Nature Geoscience*, *5*(10), 719–721. https://doi.org/10.1038/ngeo1573

MacDougall, A. H., & Knutti, R. (2016). Projecting the release of carbon from permafrost soils using a perturbed parameter ensemble modelling approach. *Biogeosciences*, *13*(7), 2123–2136. https://doi.org/10.5194/bg-13-2123-2016

Matthes, K., Funke, B., Andersson, M. E., Barnard, L., Beer, J., Charbonneau, P., Clilverd, M. A., Dudok de Wit, T., Haberreiter, M., Hendry, A., Jackman, C. H., Kretzschmar, M., Kruschke, T., Kunze, M., Langematz, U., Marsh, D. R., Maycock, A. C., Misios, S., Rodger, C. J., … Versick, S. (2017). Solar forcing for CMIP6 (v3.2). *Geoscientific Model Development*, *10*(6), 2247–2302. https://doi.org/10.5194/gmd-10-2247-2017

Mavrovic, A., Sonnentag, O., Lemmetyinen, J., Baltzer, J., Kinnard, C., & Roy, A. (2023). Reviews and syntheses: Recent advances in microwave remote sensing in support of arctic-boreal carbon cycle science. *EGUsphere*, 1–52. https://doi.org/10.5194/egusphere-2023-137

McGuire, A. D., Koven, C., Lawrence, D. M., Clein, J. S., Xia, J., Beer, C., Burke, E., Chen, G., Chen, X., Delire, C., Jafarov, E., MacDougall, A. H., Marchenko, S., Nicolsky, D., Peng, S., Rinke, A., Saito, K., Zhang, W., Alkama, R., … Zhuang, Q. (2016). Variability in the sensitivity among model simulations of permafrost and carbon dynamics in the permafrost region between 1960 and 2009. *Global Biogeochemical Cycles*, *30*(7), 1015–1037. https://doi.org/10.1002/2016GB005405

McGuire, A. D., Lawrence, D. M., Koven, C., Clein, J. S., Burke, E., Chen, G., Jafarov, E., MacDougall, A. H., Marchenko, S., Nicolsky, D., Peng, S., Rinke, A., Ciais, P., Gouttevin, I., Hayes, D. J., Ji, D., Krinner, G., Moore, J. C., Romanovsky, V., … Zhuang, Q. (2018). Dependence of the evolution of carbon dynamics in the northern permafrost region on the trajectory of climate change. *Proceedings of the National Academy of Sciences*, *115*(15), 3882–3887. https://doi.org/10.1073/pnas.1719903115

Meinshausen, M., Lewis, J., McGlade, C., Gütschow, J., Nicholls, Z., Burdon, R., Cozzi, L., & Hackmann, B. (2022). Realization of Paris Agreement pledges may limit warming just below 2 °C. *Nature*, *604*(7905), Article 7905. https://doi.org/10.1038/s41586-022-04553-z

Meinshausen, M., Nicholls, Z. R. J., Lewis, J., Gidden, M. J., Vogel, E., Freund, M., Beyerle, U., Gessner, C., Nauels, A., Bauer, N., Canadell, J. G., Daniel, J. S., John, A., Krummel, P. B., Luderer, G., Meinshausen, N., Montzka, S. A., Rayner, P. J., Reimann, S., … Wang, R. H. J. (2020). The shared socio-economic pathway (SSP) greenhouse gas concentrations and their extensions to 2500. *Geoscientific Model Development*, *13*(8), 3571–3605. https://doi.org/10.5194/gmd-13-3571-2020

Meinshausen, M., Vogel, E., Nauels, A., Lorbacher, K., Meinshausen, N., Etheridge, D. M., Fraser, P. J., Montzka, S. A., Rayner, P. J., Trudinger, C. M., Krummel, P. B., Beyerle, U., Canadell, J. G., Daniel, J. S., Enting, I. G., Law, R. M., Lunder, C. R., O'Doherty, S., Prinn, R. G., … Weiss, R. (2017). Historical greenhouse gas concentrations for climate modelling (CMIP6). *Geoscientific Model Development*, *10*(5), 2057–2116. https://doi.org/10.5194/gmd-10-2057-2017

Meissner, K. J., Weaver, A. J., Matthews, H. D., & Cox, P. M. (2003). The role of land surface dynamics in glacial inception: A study with the UVic Earth System Model. *Climate Dynamics*, *21*(7), 515–537. https://doi.org/10.1007/s00382-003-0352-2

Mekonnen, Z. A., Riley, W. J., Berner, L. T., Bouskill, N. J., Torn, M. S., Iwahana, G., Breen, A. L., Myers-Smith, I. H., Criado, M. G., Liu, Y., Euskirchen, E. S., Goetz, S. J., Mack, M. C., & Grant, R. F. (2021). Arctic tundra shrubification: A review of mechanisms and impacts on ecosystem carbon balance. *Environmental Research Letters*, *16*(5), 053001. https://doi.org/10.1088/1748-9326/abf28b

Mekonnen, Z. A., Riley, W. J., & Grant, R. F. (2018). Accelerated Nutrient Cycling and Increased Light Competition Will Lead to 21st Century Shrub Expansion in North American Arctic Tundra. *Journal of Geophysical Research: Biogeosciences*, *123*(5), 1683–1701. https://doi.org/10.1029/2017JG004319

Melnikova, I., Boucher, O., Cadule, P., Ciais, P., Gasser, T., Quilcaille, Y., Shiogama, H., Tachiiri, K., Yokohata, T., & Tanaka, K. (2021). Carbon Cycle Response to Temperature Overshoot Beyond 2°C: An Analysis of CMIP6 Models. *Earth's Future*, *9*(5), e2020EF001967. https://doi.org/10.1029/2020EF001967

Mengel, M., Nauels, A., Rogelj, J., & Schleussner, C.-F. (2018). Committed sea-level rise under the Paris Agreement and the legacy of delayed mitigation action. *Nature Communications*, *9*(1), Article 1. https://doi.org/10.1038/s41467-018-02985-8

Mengis, N., Keller, D. P., MacDougall, A. H., Eby, M., Wright, N., Meissner, K. J., Oschlies, A., Schmittner, A., MacIsaac, A. J., Matthews, H. D., & Zickfeld, K. (2020). Evaluation of the University of Victoria Earth System Climate Model version 2.10 (UVic ESCM 2.10). *Geoscientific Model Development*, *13*(9), 4183–4204. https://doi.org/10.5194/gmd-13-4183-2020

Miner, K. R., Turetsky, M. R., Malina, E., Bartsch, A., Tamminen, J., McGuire, A. D., Fix, A., Sweeney, C., Elder, C. D., & Miller, C. E. (2022). Permafrost carbon emissions in a changing Arctic. *Nature Reviews Earth & Environment*, *3*(1), Article 1. https://doi.org/10.1038/s43017-021-00230-3

Mishra, U., Hugelius, G., Shelef, E., Yang, Y., Strauss, J., Lupachev, A., Harden, J. W., Jastrow, J. D., Ping, C.-L., Riley, W. J., Schuur, E. A. G., Matamala, R., Siewert, M., Nave, L. E., Koven, C. D., Fuchs, M., Palmtag, J., Kuhry, P., Treat, C. C., … Orr, A. (2021). Spatial heterogeneity and environmental predictors of permafrost region soil organic carbon stocks. *Science Advances*, *7*(9), eaaz5236. https://doi.org/10.1126/sciadv.aaz5236

Mishra, U., Jastrow, J. D., Matamala, R., Hugelius, G., Koven, C. D., Harden, J. W., Ping, C. L., Michaelson, G. J., Fan, Z., Miller, R. M., McGuire, A. D., Tarnocai, C., Kuhry, P., Riley, W. J., Schaefer, K., Schuur, E. A. G., Jorgenson, M. T., & Hinzman, L. D. (2013). Empirical estimates to reduce modeling uncertainties of soil organic carbon in permafrost regions: A review of recent progress and remaining challenges. *Environmental Research Letters*, *8*(3), 035020. https://doi.org/10.1088/1748-9326/8/3/035020

Natali, S. M., Holdren, J. P., Rogers, B. M., Treharne, R., Duffy, P. B., Pomerance, R., & MacDonald, E. (2021). Permafrost carbon feedbacks threaten global climate goals. *Proceedings of the National Academy of Sciences*, *118*(21). https://doi.org/10.1073/pnas.2100163118

Nissan, A., Alcolombri, U., Peleg, N., Galili, N., Jimenez-Martinez, J., Molnar, P., & Holzner, M. (2023). Global warming accelerates soil heterotrophic respiration. *Nature Communications*, *14*(1), Article 1. https://doi.org/10.1038/s41467-023-38981-w

Nzotungicimpaye, C.-M., & Zickfeld, K. (2017). The Contribution from Methane to the Permafrost Carbon Feedback. *Current Climate Change Reports*, *3*(1), 58–68. https://doi.org/10.1007/s40641-017-0054-1

Nzotungicimpaye, C.-M., Zickfeld, K., MacDougall, A. H., Melton, J. R., Treat, C. C., Eby, M., & Lesack, L. F. W. (2021). WETMETH 1.0: A new wetland methane model for implementation in Earth system models. *Geoscientific Model Development*, *14*(10), 6215–6240. https://doi.org/10.5194/gmd-14-6215-2021

O'Neill, B. C., Tebaldi, C., van Vuuren, D. P., Eyring, V., Friedlingstein, P., Hurtt, G., Knutti, R., Kriegler, E., Lamarque, J.-F., Lowe, J., Meehl, G. A., Moss, R., Riahi, K., & Sanderson, B. M. (2016). The Scenario Model Intercomparison Project (ScenarioMIP) for CMIP6. *Geoscientific Model Development*, *9*(9), 3461–3482. https://doi.org/10.5194/gmd-9-3461-2016

Pacanowski, R. C. (1996). Documentation user's guide and reference manual (MOM2, Version 2). *GFDL Ocean Technical Report 3.2*, *329*. https://ci.nii.ac.jp/naid/10010166546/

Park, S.-W., & Kug, J.-S. (2022). A decline in atmospheric CO2 levels under negative emissions may enhance carbon retention in the terrestrial biosphere. *Communications Earth & Environment*, *3*(1), Article 1. https://doi.org/10.1038/s43247-022-00621-4

Qiu, H., Hao, D., Zeng, Y., Zhang, X., & Chen, M. (2023). Global and northern-high-latitude net ecosystem production in the 21st century from CMIP6 experiments. *Earth System Dynamics*, *14*(1), 1–16. https://doi.org/10.5194/esd-14-1-2023

Riahi, K., van Vuuren, D. P., Kriegler, E., Edmonds, J., O'Neill, B. C., Fujimori, S., Bauer, N., Calvin, K., Dellink, R., Fricko, O., Lutz, W., Popp, A., Cuaresma, J. C., Kc, S., Leimbach, M., Jiang, L., Kram, T., Rao, S., Emmerling, J., … Tavoni, M. (2017). The Shared Socioeconomic Pathways and their energy, land use, and greenhouse gas emissions implications: An overview. *Global Environmental Change*, *42*, 153–168. https://doi.org/10.1016/j.gloenvcha.2016.05.009

Rogelj, J., Popp, A., Calvin, K. V., Luderer, G., Emmerling, J., Gernaat, D., Fujimori, S., Strefler, J., Hasegawa, T., Marangoni, G., Krey, V., Kriegler, E., Riahi, K., van Vuuren, D. P., Doelman, J., Drouet, L., Edmonds, J., Fricko, O., Harmsen, M., … Tavoni, M. (2018). Scenarios towards limiting global mean temperature increase below 1.5 °C. *Nature Climate Change*, *8*(4), Article 4. https://doi.org/10.1038/s41558-018-0091-3

Saunois, M., Stavert, A. R., Poulter, B., Bousquet, P., Canadell, J. G., Jackson, R. B., Raymond, P. A., Dlugokencky, E. J., Houweling, S., Patra, P. K., Ciais, P., Arora, V. K., Bastviken, D., Bergamaschi, P., Blake, D. R., Brailsford, G., Bruhwiler, L., Carlson, K. M., Carrol, M., … Zhuang, Q. (2020). The Global Methane Budget 2000–2017. *Earth System Science Data*, *12*(3), 1561–1623. https://doi.org/10.5194/essd-12-1561-2020

Schädel, C., Bader, M. K.-F., Schuur, E. A. G., Biasi, C., Bracho, R., Čapek, P., De Baets, S., Diáková, K., Ernakovich, J., Estop-Aragones, C., Graham, D. E., Hartley, I. P., Iversen, C. M., Kane, E., Knoblauch, C., Lupascu, M., Martikainen, P. J., Natali, S. M., Norby, R. J., … Wickland, K. P. (2016). Potential carbon emissions dominated by carbon dioxide from thawed permafrost soils. *Nature Climate Change*, *6*(10), Article 10. https://doi.org/10.1038/nclimate3054

Schmittner, A., Oschlies, A., Matthews, H. D., & Galbraith, E. D. (2008). Future changes in climate, ocean circulation, ecosystems, and biogeochemical cycling simulated for a business-as-usual CO2 emission scenario until year 4000 AD. *Global Biogeochemical Cycles*, *22*(1). https://doi.org/10.1029/2007GB002953

Schuur, E. A. G., Abbott, B. W., Commane, R., Ernakovich, J., Euskirchen, E., Hugelius, G., Grosse, G., Jones, M., Koven, C., Leshyk, V., Lawrence, D., Loranty, M. M., Mauritz, M., Olefeldt, D., Natali, S., Rodenhizer, H., Salmon, V., Schädel, C., Strauss, J., … Turetsky, M. (2022). Permafrost and Climate Change: Carbon Cycle Feedbacks From the Warming Arctic. *Annual Review of Environment and Resources*, *47*(1), 343–371. https://doi.org/10.1146/annurev-environ-012220-011847

Schuur, E. A. G., McGuire, A. D., Schädel, C., Grosse, G., Harden, J. W., Hayes, D. J., Hugelius, G., Koven, C. D., Kuhry, P., Lawrence, D. M., Natali, S. M., Olefeldt, D., Romanovsky, V. E., Schaefer, K., Turetsky, M. R., Treat, C. C., & Vonk, J. E. (2015). Climate change and the permafrost carbon feedback. *Nature*, *520*(7546), 171–179. https://doi.org/10.1038/nature14338

Schwinger, J., Asaadi, A., Steinert, N. J., & Lee, H. (2022). Emit now, mitigate later? Earth system reversibility under overshoots of different magnitude and duration. *Earth System Dynamics Discussions*, 1–34. https://doi.org/10.5194/esd-2022-39

Sgubin, G., Swingedouw, D., Drijfhout, S., Hagemann, S., & Robertson, E. (2015). Multimodel analysis on the response of the AMOC under an increase of radiative forcing and its symmetrical reversal. *Climate Dynamics*, *45*(5), 1429–1450. https://doi.org/10.1007/s00382-014-2391-2

Shakhova, N., Semiletov, I., Sergienko, V., Lobkovsky, L., Yusupov, V., Salyuk, A., Salomatin, A., Chernykh, D., Kosmach, D., Panteleev, G., Nicolsky, D., Samarkin, V., Joye, S., Charkin, A., Dudarev, O., Meluzov, A., & Gustafsson, O. (2015). The East Siberian Arctic Shelf: Towards further assessment of permafrost-related methane fluxes and role of sea ice. *Philosophical Transactions of the Royal Society A: Mathematical, Physical and Engineering Sciences*, *373*(2052), 20140451. https://doi.org/10.1098/rsta.2014.0451

Shu, S., Jain, A. K., Koven, C. D., & Mishra, U. (2020). Estimation of Permafrost SOC Stock and Turnover Time Using a Land Surface Model With Vertical Heterogeneity of Permafrost Soils. *Global Biogeochemical Cycles*, *34*(11), e2020GB006585. https://doi.org/10.1029/2020GB006585

Smith, C. J., Forster, P. M., Allen, M., Fuglestvedt, J., Millar, R. J., Rogelj, J., & Zickfeld, K. (2019). Current fossil fuel infrastructure does not yet commit us to 1.5 °C warming. *Nature Communications*, *10*(1), 101. https://doi.org/10.1038/s41467-018-07999-w

Smith, P., Davis, S. J., Creutzig, F., Fuss, S., Minx, J., Gabrielle, B., Kato, E., Jackson, R. B., Cowie, A., Kriegler, E., van Vuuren, D. P., Rogelj, J., Ciais, P., Milne, J., Canadell, J. G., McCollum, D., Peters, G., Andrew, R., Krey, V., … Yongsung, C. (2016). Biophysical and economic limits to negative CO2 emissions. *Nature Climate Change*, *6*(1), 42–50. https://doi.org/10.1038/nclimate2870

Strauss, J., Schirrmeister, L., Grosse, G., Fortier, D., Hugelius, G., Knoblauch, C., Romanovsky, V., Schädel, C., Schneider von Deimling, T., Schuur, E. A. G., Shmelev, D., Ulrich, M., & Veremeeva, A. (2017). Deep Yedoma permafrost: A synthesis of depositional characteristics and carbon vulnerability. *Earth-Science Reviews*, *172*, 75–86. https://doi.org/10.1016/j.earscirev.2017.07.007

Tokarska, K. B., & Zickfeld, K. (2015). The effectiveness of net negative carbon dioxide emissions in reversing anthropogenic climate change. *Environmental Research Letters*, *10*(9), 094013. https://doi.org/10.1088/1748-9326/10/9/094013

Turetsky, M. R., Abbott, B. W., Jones, M. C., Anthony, K. W., Olefeldt, D., Schuur, E. A. G., Grosse, G., Kuhry, P., Hugelius, G., Koven, C., Lawrence, D. M., Gibson, C., Sannel, A. B. K., & McGuire, A. D. (2020). Carbon release through abrupt permafrost thaw. *Nature Geoscience*, *13*(2), Article 2. https://doi.org/10.1038/s41561-019-0526-0

UNFCCC. (2015). *Adoption of the Paris Agreement*.

UNFCCC. (2021). Glasgow Climate Pact. *United Nations Framework Convention on Climate Change*. https://unfccc.int/documents/310475

Varney, R. M., Chadburn, S. E., Burke, E. J., & Cox, P. M. (2022). Evaluation of soil carbon simulation in CMIP6 Earth system models. *Biogeosciences*, *19*(19), 4671–4704. https://doi.org/10.5194/bg-19-4671-2022

Walter Anthony, K., Schneider von Deimling, T., Nitze, I., Frolking, S., Emond, A., Daanen, R., Anthony, P., Lindgren, P., Jones, B., & Grosse, G. (2018). 21st-century modeled permafrost carbon emissions accelerated by abrupt thaw beneath lakes. *Nature Communications*, *9*(1), Article 1. https://doi.org/10.1038/s41467-018-05738-9

Wang, K., Zhang, T., & Clow, G. D. (2023). Permafrost Thermal Responses to Asymmetrical Climate Changes: An Integrated Perspective. *Geophysical Research Letters*, *50*(5), e2022GL100327. https://doi.org/10.1029/2022GL100327

Warner, D. L., Bond-Lamberty, B., Jian, J., Stell, E., & Vargas, R. (2019). Spatial Predictions and Associated Uncertainty of Annual Soil Respiration at the Global Scale. *Global Biogeochemical Cycles*, *33*(12), 1733–1745. https://doi.org/10.1029/2019GB006264

Watts, J. D., Natali, S. M., Minions, C., Risk, D., Arndt, K., Zona, D., Euskirchen, E. S., Rocha, A. V., Sonnentag, O., Helbig, M., Kalhori, A., Oechel, W., Ikawa, H., Ueyama, M., Suzuki, R., Kobayashi, H., Celis, G., Schuur, E. A. G., Humphreys, E., … Edgar, C. (2021). Soil respiration strongly offsets carbon uptake in Alaska and Northwest Canada. *Environmental Research Letters*, *16*(8), 084051. https://doi.org/10.1088/1748-9326/ac1222

Weaver, A. J., Eby, M., Wiebe, E. C., Bitz, C. M., Duffy, P. B., Ewen, T. L., Fanning, A. F., Holland, M. M., MacFadyen, A., Matthews, H. D., Meissner, K. J., Saenko, O., Schmittner, A., Wang, H., & Yoshimori, M. (2001). The UVic earth system climate model: Model description, climatology, and applications to past, present and future climates. *Atmosphere-Ocean*, *39*(4), 361–428. https://doi.org/10.1080/07055900.2001.9649686

Wright, N. (2020). *Projected changes in Northern Hemisphere permafrost in temperature stabilization and overshoot scenarios* [MSc Thesis, Simon Fraser University]. https://summit.sfu.ca/item/19828

Zhu, D., Ciais, P., Krinner, G., Maignan, F., Jornet Puig, A., & Hugelius, G. (2019). Controls of soil organic matter on soil thermal dynamics in the northern high latitudes. *Nature Communications*, *10*(1), Article 1. https://doi.org/10.1038/s41467-019-11103-1

Zickfeld, K., MacDougall, A. H., & Matthews, H. D. (2016). On the proportionality between global temperature change and cumulative CO_2 emissions during periods of net negative CO_2 emissions. *Environmental Research Letters*, *11*(5), 055006. https://doi.org/10.1088/1748-9326/11/5/055006

Appendix. Supplementary Figures

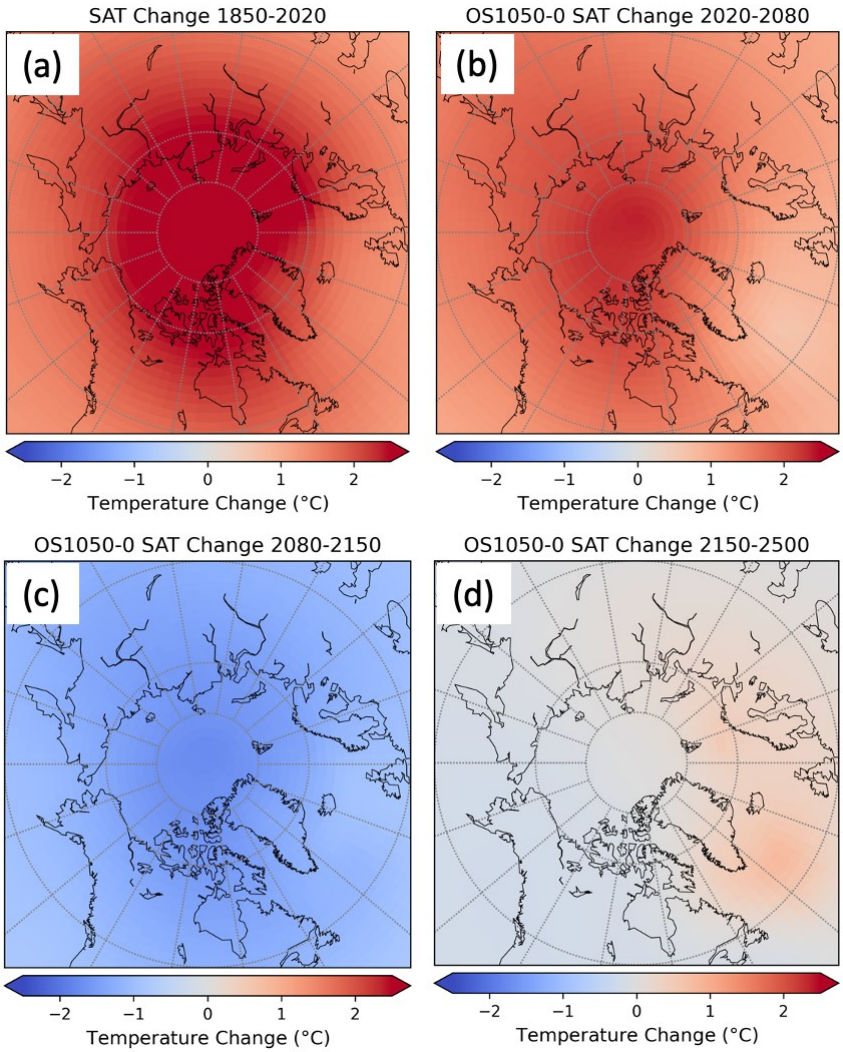

Figure A1 **Spatial plots of surface air temperature change in the northern high-latitude grid cells between a)1850-2020, b)2020-2080, c)2080-2150, d)2150-2500**

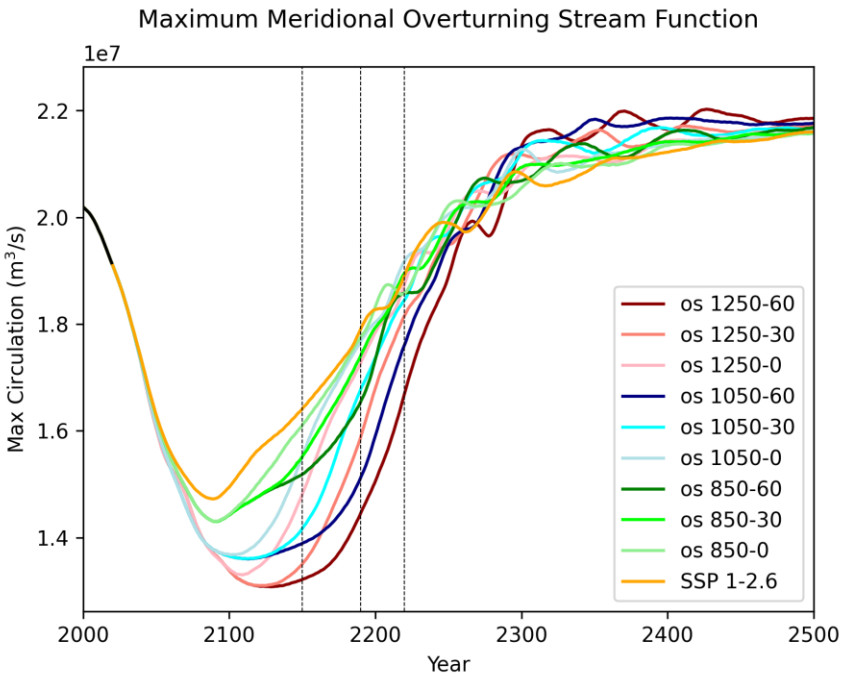

Figure A2 **Maximum Meridional Overturning Circulation for each of the overshoot scenarios**

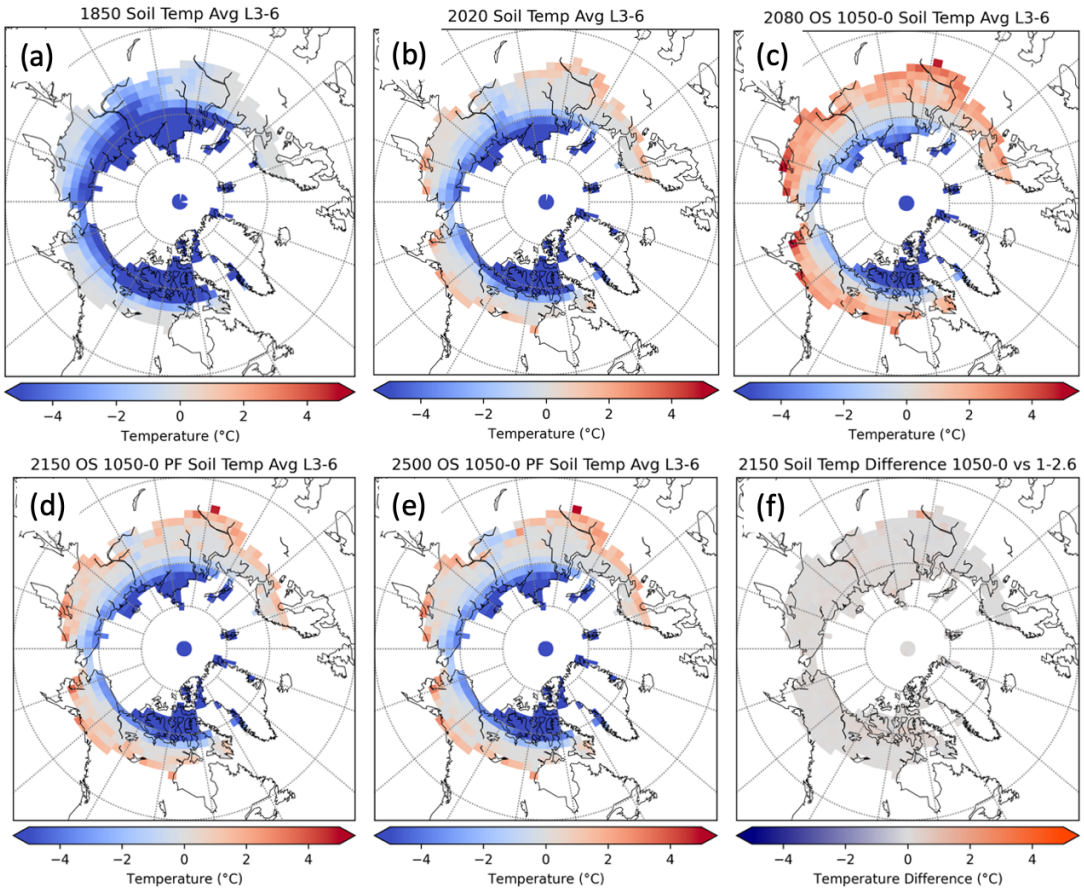

Figure A3 **Absolute soil temperature for key years between 1850 and 2500 in OS1050-0. Each plot shows the average soil temperature between the depth of 0.27-3.35m in layers 3-6 (the four layers that contain permafrost carbon). a) 1850, b)2020, c)2080, d)2150, e)2500. F) Average soil temperature difference for layers 3-6 between OS1050-0 and SSP1-2.6 in 2150**

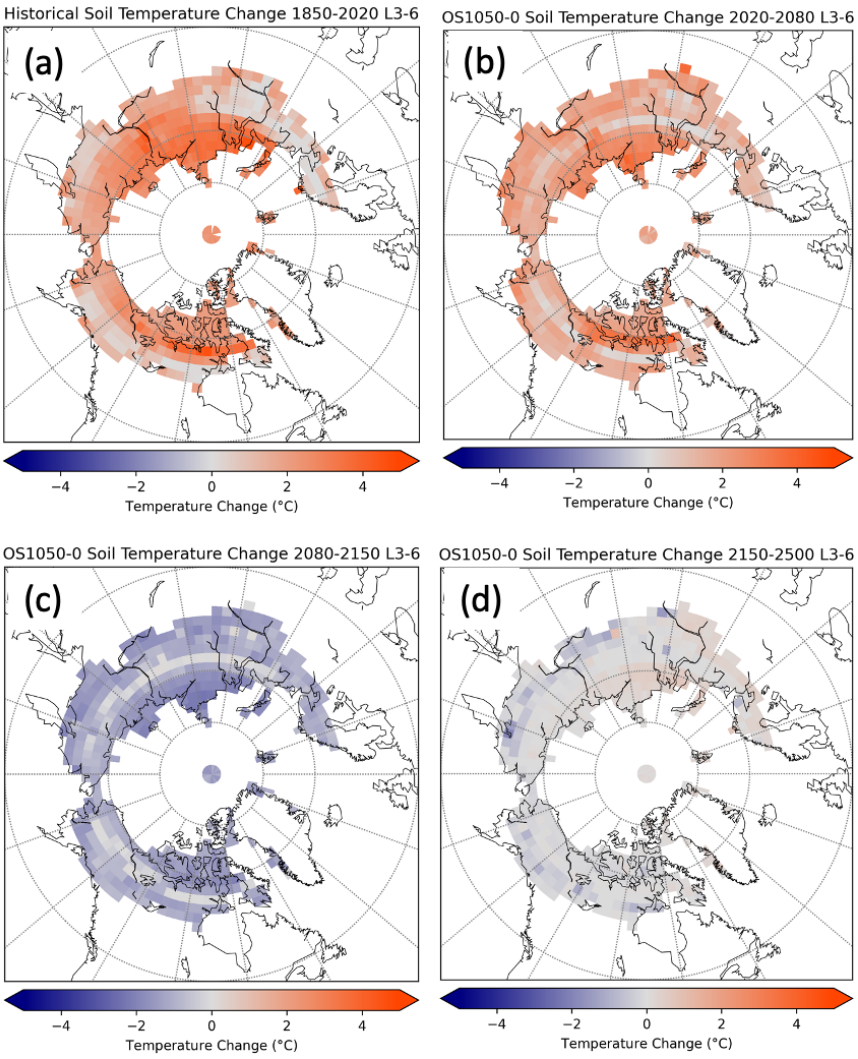

Figure A4 **Soil temperature evolution between 1850-2500 for OS1050-0. Each panel shows the temperature change relative to the previous key year. Each grid cell is the average temperature change for layers 3-6 (the four layers that contain permafrost carbon).**

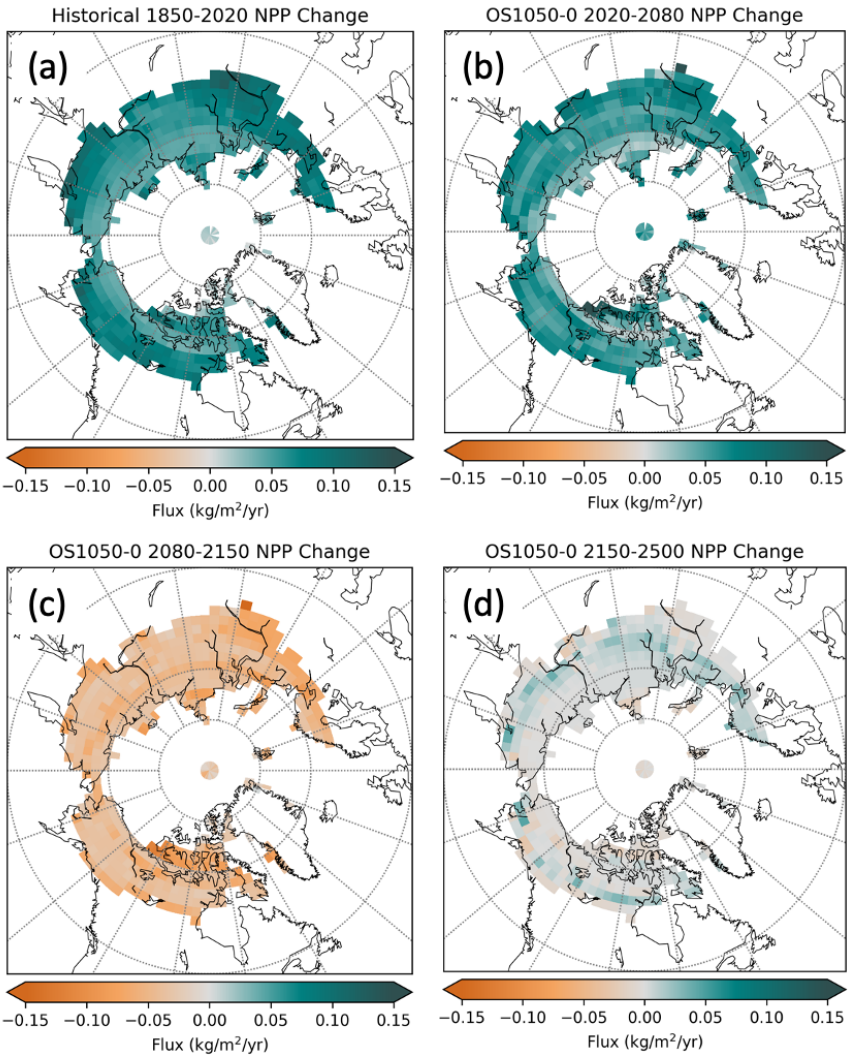

Figure A5 **Change in net primary productivity (NPP) for all plant functional types in permafrost carbon grid cells.**

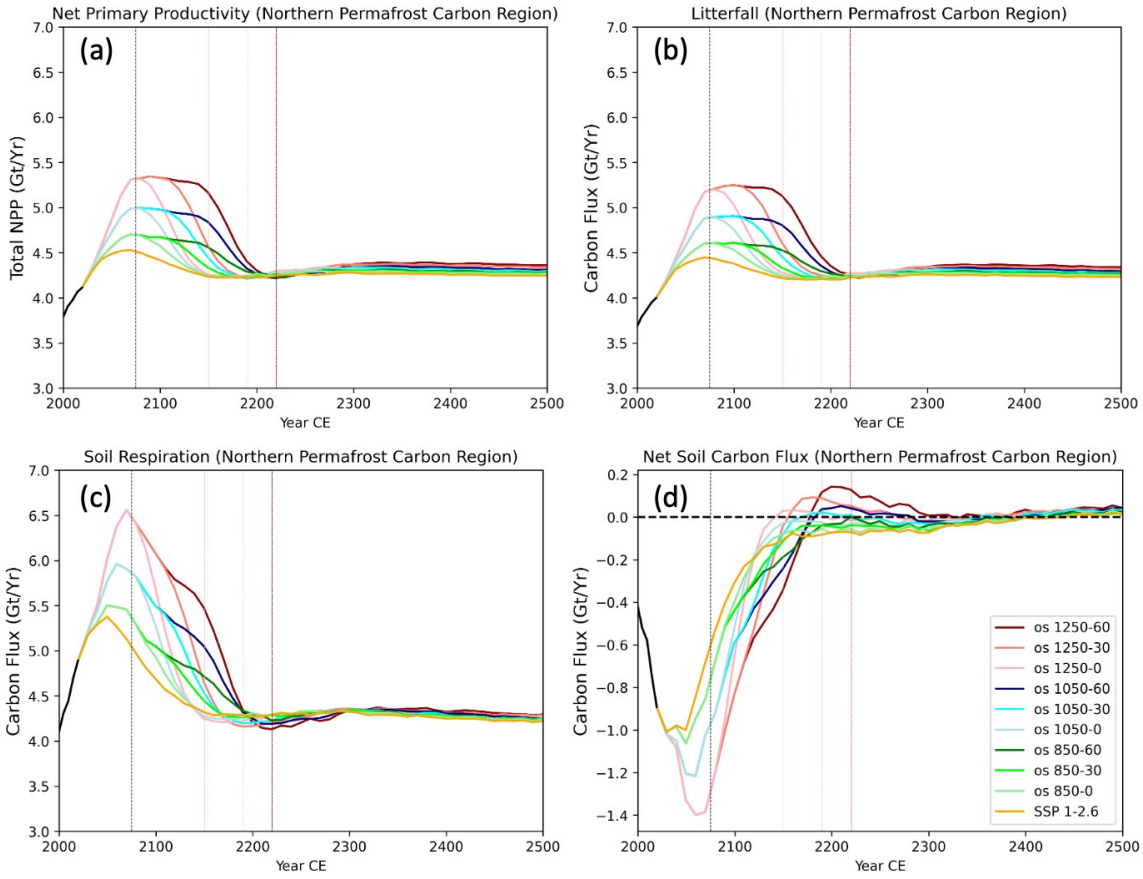

Figure A6 **Time series of land carbon fluxes within the northern high-latitude permafrost region. a) Net primary productivity, b) litterfall flux, c) soil respiration, d) net balance between vegetation litter and soil respiration. In d), a positive flux indicates soil carbon gain, and a negative flux indicates soil carbon loss to the atmosphere. The black dotted vertical line at 2075 indicates the peak cumulative carbon emission year, and the coloured vertical lines indicate the years the OS scenario cumulative CO_2 emissions converge with those in SSP1-2.6: years 2150, 2190, and 2220 for scenarios with 0, 30 and 60 years overshoot duration, respectively.**

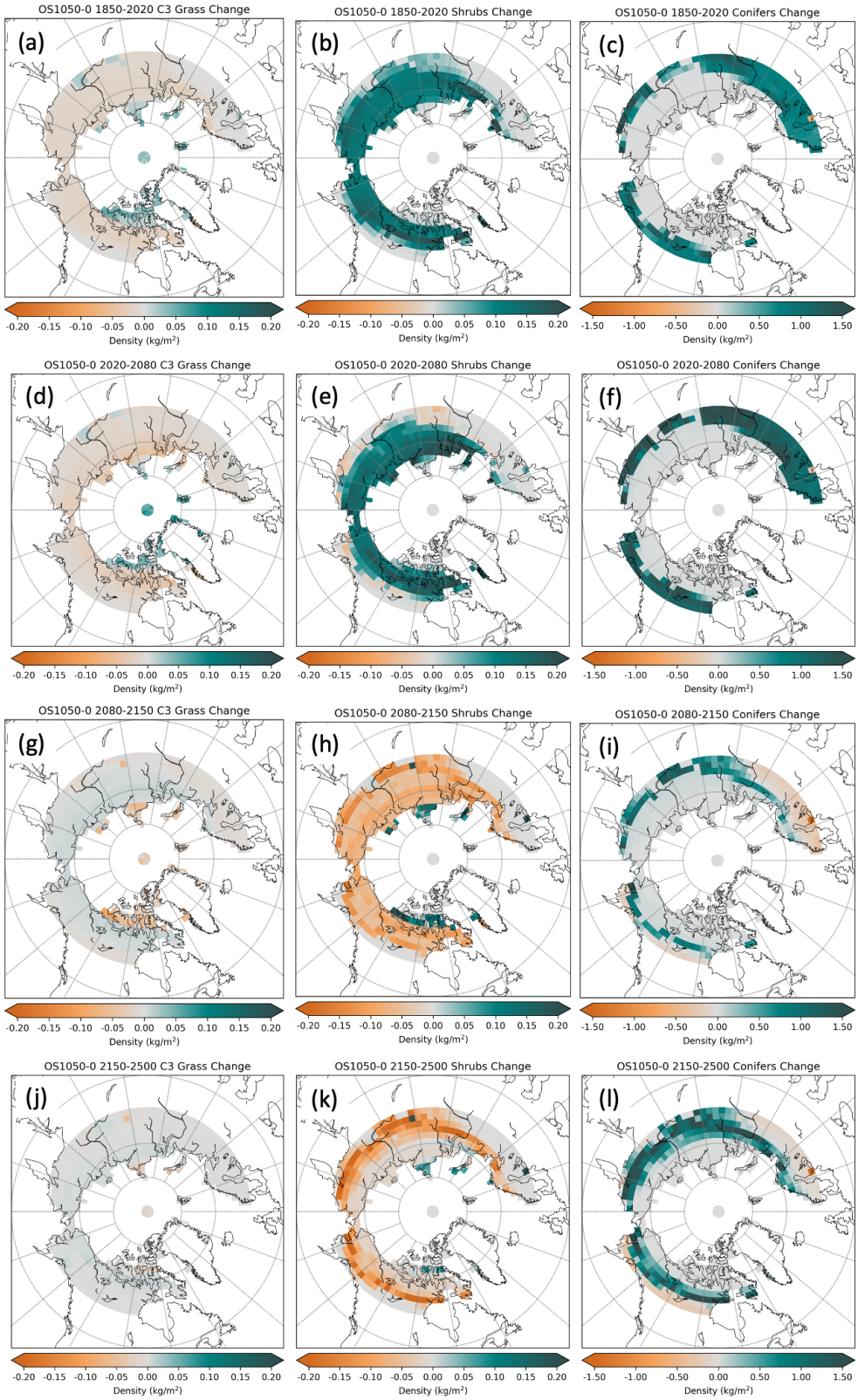

Figure A7 **Vegetation carbon density change for each of the plant functional types present in the northern high-latitudes. Note that the density scale is different for coniferous trees.**

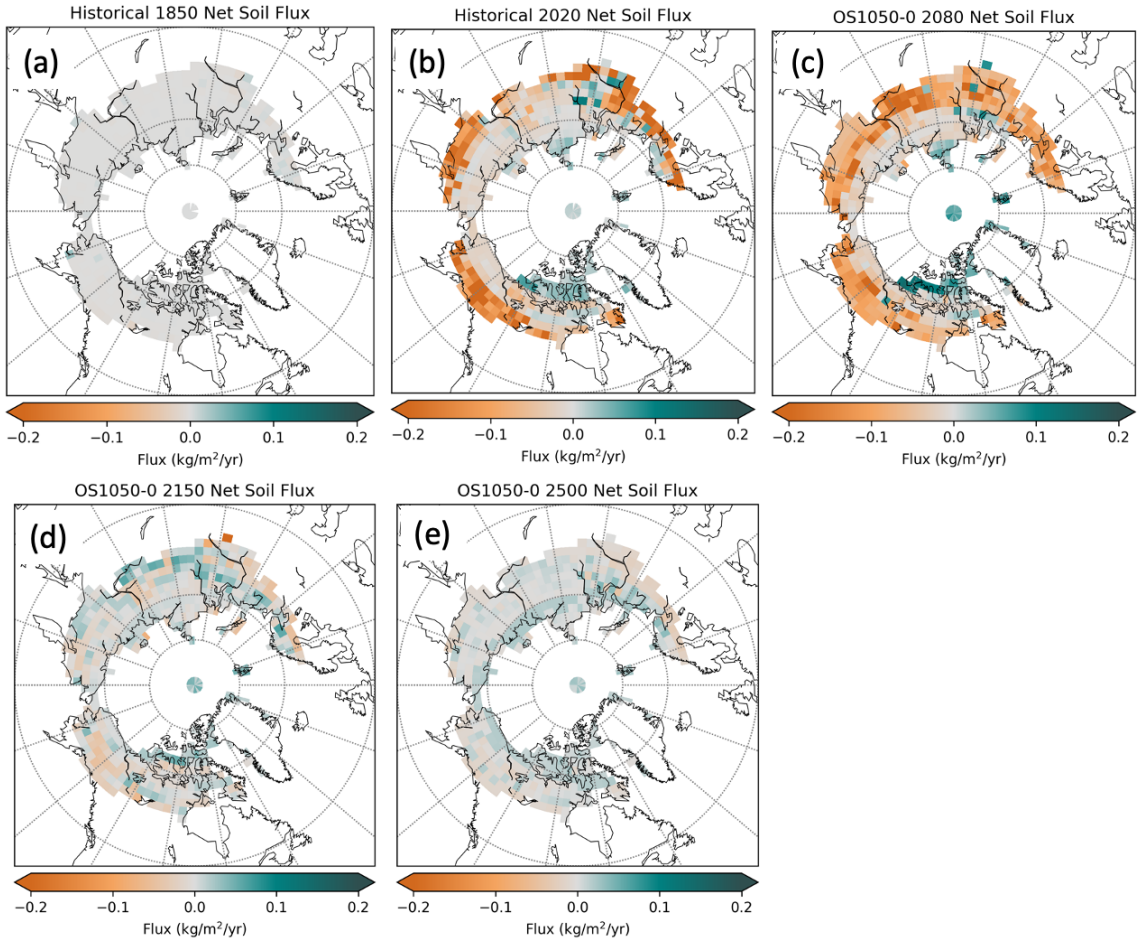

Figure A8 **Net soil carbon balance between vegetation litter (input) and soil respiration (output). A positive flux indicates soil carbon gain, and a negative flux indicates soil carbon loss to the atmosphere. These are spatial snapshots of Figure A6d.**

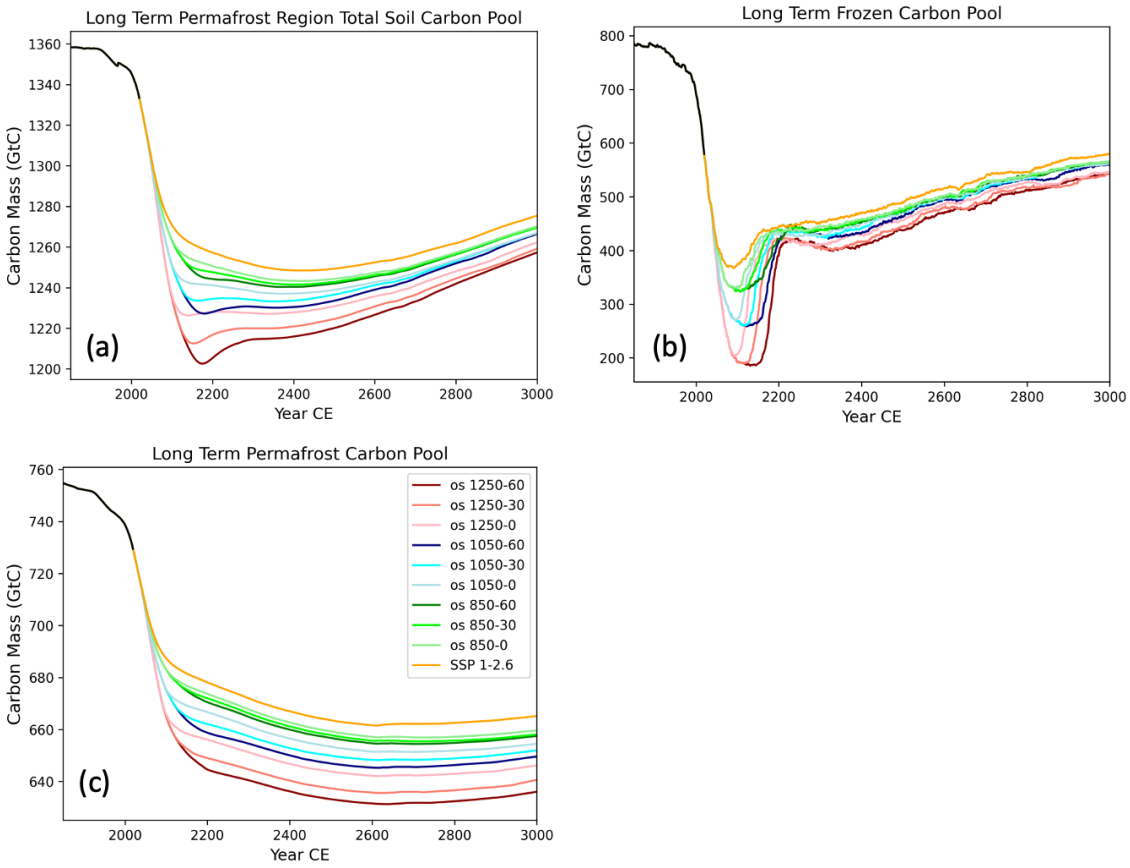

Figure A9 **Long-term time series of a) total unfrozen and frozen soil carbon pool within the permafrost region, b) total carbon contained only within frozen soils, c) total permafrost carbon accumulated through the diffusive mixing process. Same as Figure 4b-d but shows the reversibility timeline until 3000 CE.**